Netherlands Journal of Sea Research
33 (3/4): 453-483 (1995)

BENTHIC NUTRIENT REGENERATION IN THE ERSEM ECOSYSTEM MODEL OF THE NORTH SEA *

PIET RUARDIJ & WIM VAN RAAPHORST

Netherlands Institute for Sea Research, P.O. Box 59, NL-1790 AB Den Burg, Texel, The Netherlands

ABSTRACT

In any ecosystem modelling approach to shallow seas an adequate description of the sediment-water interactions to all the essential nutrients is necessary. With this aim a fairly simple concept has been developed and applied for the modelling of the nutrient cycles of N, P and Si which includes the essential diagenetic processes such as vertical transport, oxic and anoxic mineralization, silicate dissolution, adsorption, nitrification and denitrification. All these processes are explicitly formulated for one or more distinct layers in the sediment. The model contains a low number of variables and is efficient with respect to computer time. The model is part of the European Regional Seas Ecosystem Model (ERSEM) of the North Sea, a joint effort of several institutes around the North Sea. The benthic-pelagic coupling of the ERSEM model is discussed with emphasis on the consequences for the benthic nutrient cycling and the interrelations between the different benthic nutrient submodels. The results show that the model is able to describe the seasonal variation of nutrient fluxes including the sediment-water exchanges and the vertical profiles in the pore water. From the model results is concluded that changes in organic matter deposition directly influence the benthic nitrification and denitrification through changes in the oxygen availability to the nitrifiers and, due to this, the supply of nitrate to the denitrifiers. Short fluctuations in organic deposition (*e.g.* after the spring bloom) are not reflected in the fluxes due to sorption buffering of phosphate in the oxidized surface layer of the sediment.

1. INTRODUCTION

In shallow seas the sediment-water exchange is often an essential nutrient source for primary producers. The reduction of external nutrient inputs may be counteracted by benthic nutrient release, particularly when the sediments have high nutrient contents. In all regional sea ecosystems nutrients limit the primary production during most of the season and therefore the sediment-water interaction (pelagic-benthic coupling) is an essential process.

The ERSEM model (European Regional Seas Ecosystem Model), a joint effort of nine institutes around the North Sea (Baretta *et al.*, 1995) includes chemical, biological and physical processes. In the model the North Sea is subdivided into ten boxes (Fig. 1) in a similar way as by ICES (International Council for Exploration of the Sea). The water column of the five boxes in the northern part that are stratified during summer is further subdivided into an upper and a lower box. The model includes a description of the pelagic (Varela *et al.*, 1995; Baretta-Bekker *et al.*, 1995; Broekhuizen *et al.*, 1995) and the benthic system (Ebenhöh *et al.*, 1995). The transport between the (large) boxes is based on the hydrodynamical model described by Lenhart *et al.* (1995). Here we present the cycling and regeneration of nutrients in the sediments (Fig. 2).

Diagenetic processes in the sediment control the fluxes at the sediment-water interface and as such are an essential part of the ecosystem. Benthic nutrient models as separate models or as part of an ecosystem model have not often been applied in the past to shelf seas such as the North Sea. Until now the ecological modelling of the North Sea has been mainly limited to the pelagic and transport processes (Fransz *et al.*, 1991). For tidal areas diagenetic processes of phosphate have been included in a complex ecosystem model (Van Raaphorst *et al.*, 1988). Models have been used, however, for studying the processes involved in sediment-water interactions in North Sea sediments. For example Billen (1982) and Van Raap-

*Publication no. 67 of the project: Applied Scientific Research, Netherlands Institute for Sea Research (BEWON).

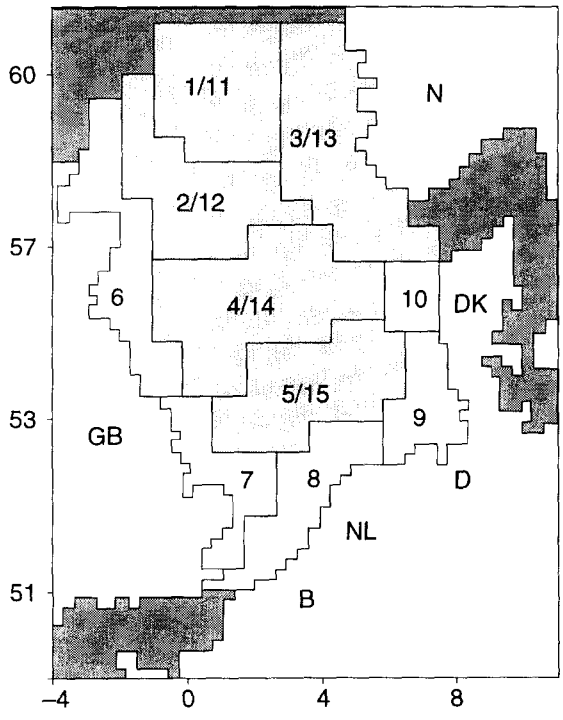

Fig. 1. Division of the North Sea into large-scale boxes, similar to the ICES boxes. Only the ICES box in the German Bight and along the Danish coast is divided into a small northern (10) and a large southern box (9). The coastal boxes are 6 to 10. The deep boxes are divided into upper boxes of 30 m depth (boxes 1 to 5) and lower boxes from 30 m down to the bottom (boxes 11 to 15). The boxes in which stratification occurs during summer are shaded.

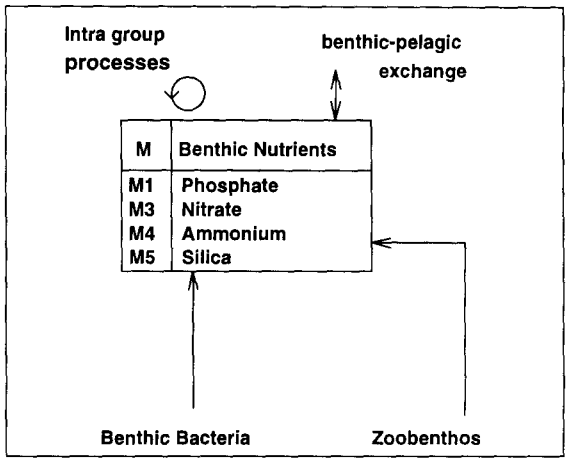

Fig. 2. Detail of the ERSEM process flow diagram (fig. 3. of Blackford & Radford, 1995) showing the forcing of the model (mineralization by bacteria and zoobenthos and the exchange with the overlying water); all vertical transports and within sediment are summarized as intragroup processes.

horst *et al.* (1990) applied steady-state solutions of a set of partial differential equations to analyse their observed pore-water profiles.

In the literature many formulations for benthic fluxes can be found, ranging from purely empirical relationships to formal and theoretical models (Aller, 1980; Berner, 1980; Jahnke *et al.*, 1982; Van Raaphorst *et al.*, 1990). The ERSEM model is deterministic and aims at completeness. Thus the formal approach seems the most appropriate. As a consequence, all the relevant processes should be described explicitly, giving rise to a large number of state variables and parameters. Since there is a strong interaction between dissolved components and particulates, mass balances have to be set up both for the dissolved and the solid phase. This generally leads to a large set of equations that have to be solved in a large number of thin sediment layers, mostly for small timesteps. These are undesirable features in an ecosystem model in which the benthic nutrient submodel is a crucial but still small part and where the period to be simulated is mostly in the order of months to years. Aggregation of the essential processes to a simpler approach is therefore necessary. Thus the present approach concerns a conceptual model with a low number of state variables and parameters, in which only a limited amount of *a priori* knowledge of the processes dominating the benthic system is incorporated. In the paper this simplified approach is presented and analysed. In summary the aim of this study is twofold:

- to construct nutrient models for the sediments including all important early diagenetic processes for the whole North Sea and describing the direct and indirect effects of the deposition of particulate organic matter on the nutrient cycles in space and time;
- to develop and test a computationally efficient method to model the dynamical behaviour of nutrient pore-water profiles but especially nutrient fluxes.

2. BASIC CONCEPTS

The basis for our models is the general diagenetic equation developed in Berner (1980). For any component dissolved in the pore water this equation takes the form:

$$\frac{\partial \phi C}{\partial t} = \frac{\partial (\phi D \frac{\partial C}{\partial z})}{\partial z} - \frac{\partial (\phi \omega C)}{\partial z} + \phi \Sigma R \qquad (1)$$

where

C: Concentration of the component dissolved in the pore water (mmol·m^{-3}).
t: time (d).
z: depth in the sediment, zero at the sediment-water interface (m).
ϕ: volumetric porosity (-).
D: whole sediment diffusion coefficient (m^2·d^{-1}).
ω: whole sediment advection constant (m·d^{-1}).
ΣR: the sum of all reactions and transformations affecting C (mmol·m^{-3}·d^{-1}).

All parameters of Eq. 1 may vary with depth and can be a function of other components. This implies that Eq. 1 represents a set of equations coupled through the parameters. To give an example, NO_3^- production through nitrification is directly coupled to both O_2 and NH_4^+. The vertical variability of the parameters is covered in the models by schematizing the sediment into a limited number of layers. Our main objective is to adequately describe fluxes at the sediment-water interface, rather than to simulate vertical concentration profiles in great detail. Thus we refrain from using a large number of thin layers, but restrict the schematization to three functional layers: 1. the oxic layer, in which O_2 serves as main electron acceptor; 2. the denitrification layer, in which nitrate is reduced; 3. the sulphide layer, in which Mn(IV), Fe(III) and sulphate are reduced through mineralization of organic matter. In each of these layers Eq. 1 is applied with depth invariant parameters. The layers are linked by stating continuity in both concentrations and fluxes at the boundaries. The other simplifications are:

- all loss processes are modelled as first-order reactions, productions are assumed to have zero-order kinetics;
- fast adsorption is included as an instantaneous equilibrium reaction (Berner, 1976);
- advection is ignored as relatively unimportant in comparison to diffusion and the other processes concerned.

Now for each of the layers the basic equation becomes:

$$(p+1)\frac{\partial C}{\partial t} = D\frac{\partial^2 C}{\partial z^2} - kC + M \qquad (2)$$

in which:

k: first-order loss rate constant (d^{-1}).
M: zero-order production rate constant (mmol·m^{-3}·d^{-1}).
p: dimensionless distribution coefficient defined as the proportion between the concentration of the adsorbed and dissolved constituent, respectively.

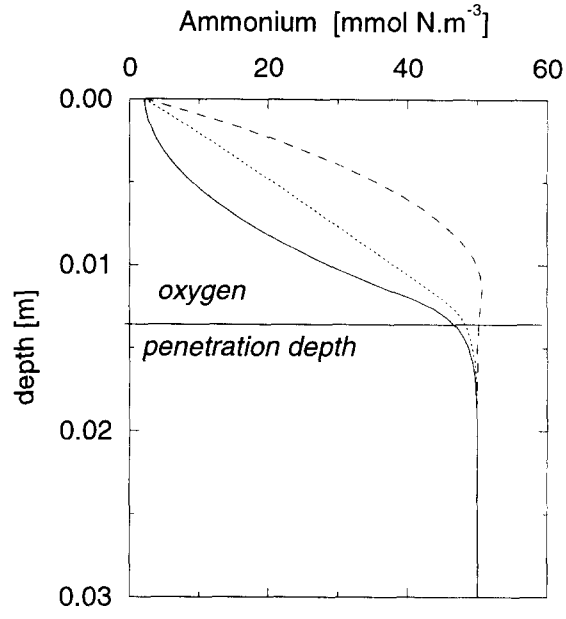

Fig. 3. An example of an initial profile P_{in} (solid line) obtained from the preceding time step, a steady state profile P_{eq} (dashed line) and a transient profile P_{tr} (dotted line) for ammonium. See text for further explanation.

3. SIMULATION OF FLUXES AND GRADIENTS

The model is based on analytical solutions of Eq. 2. Obviously, full dynamic solutions of Eq. 2 cannot always be found and the approach would then lead to serious mathematical problems. Instead we approximate the dynamical behaviour starting from steady-state solutions of Eq. 2. Subsequently we make corrections to account for the effect of changing fluxes and profiles within a time-step. This sequence (steady state, corrections) is performed every time-step of a simulation run. The steady-state solutions are obtained by standard numerical techniques (Press *et al.*, 1986) after introduction of the time-step dependent boundary conditions and parameter values. The need for correction is based on the consideration that it takes some time to reach a new steady state and that steady-state fluxes and profiles may not be established within a single time step. Consequently the steady-state fluxes do not represent time-step averaged fluxes, even when steady-state is actually reached within a time step. The average profiles and

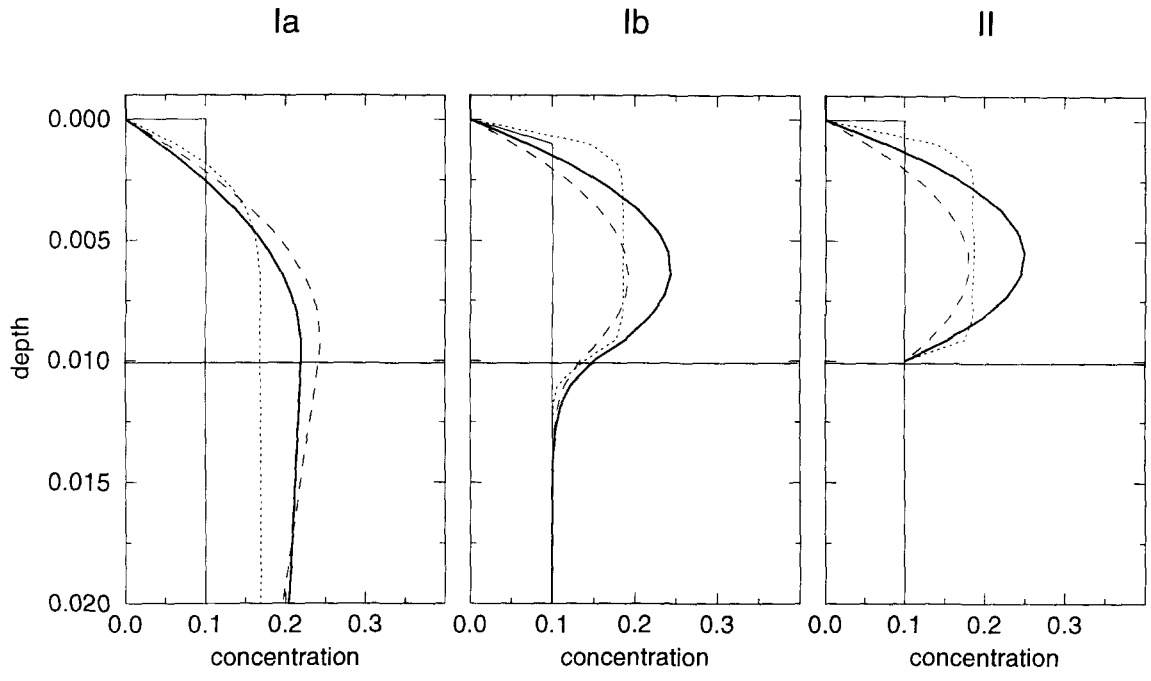

Fig. 4. The gradient after one time step in the presence of mineralization (M) and a first-order loss term with coefficient k for three cases: Ia. $M \neq 0$ in layer $0 < z < 0.1$, $k = 0$; Ib. $M \neq 0$ in layer $0 < z < 0.01$, $k = 0$; II. $M \neq 0$, $k > 0$ in layer $0 < z < 0.01$. Initial condition: $C = 0.1$ for $z > 0$. Boundary condition: $C(z) = 0$ for $z = 0$. The thin solid line represents the initial profile, the dashed line the transient profile, the thick solid line the profile after one time step, the dotted line profile calculated with the analytical solution of the dynamical equation after one time step.

hence the time-step dependent fluxes also depend on the initial profiles. To account for this we distinguish three concentration profiles for each layer (Fig. 3): 1. the initial profile (P_{in}) obtained from the preceding time step; 2. the equilibrium profile (P_{eq}) finally to be obtained at steady-state conditions and 3. the transient profile (P_{tr}) defined as the time averaged profile underway from P_{in} towards P_{eq}. The correction thus consists of calculating P_{tr} and its associated fluxes.

The calculation is done in an indirect way. The associated depth averaged concentrations $\overline{C_{in}}$ and $\overline{C_{eq}}$ are determined from P_{in} and P_{eq}, respectively, and are used to calculate $\overline{C_{tr}}$ according to:

$$\overline{C_{tr}} = \overline{C_{eq}} + (\overline{C_{in}} - \overline{C_{eq}}) \cdot (1 - e^{-\frac{\Delta t}{t_a}}) \cdot \frac{t_a}{\Delta t} \quad (3)$$

in which Δt is the time step and t_a the adaptation time.

The adaptation time (t_a) is derived from the analytical solution of the general dynamical equation and is defined as (Carslaw & Jaeger, 1946):

$$t_a = \frac{p+1}{k + \pi^2 D/H^2} \quad (4)$$

in which D is the diffusion coefficient in the layer and H is the thickness of the layer in which C is defined (Appendix A.). Subsequently, P_{tr} is calculated under the constraint that the average value of C is $\overline{C_{tr}}$.

To calculate P_{tr} we assume that changes from time step to time step are small in the deeper layers and that the shapes of the profiles within the individual layers are close to their steady state. In other words, we expect 'pseudo steady state' in the layers, but, without 'equilibrium' between the layers. Thus P_{tr} is calculated from the steady-state solutions of Eq. 2, creating a fictitious mineralization term to match $\overline{C_{tr}}$ in the upper layer and P_{in} in both lower layers. From P_{tr} the concentration gradients at the interfaces and associated fluxes are calculated, as well as all first-order loss processes. Subtracting the fluxes and losses from the original and true mineralization yields the total change $\overline{\Delta C}$ in the layers. This value is transferred to the integration subroutine of the simulation package for the calculation of the next $\overline{C_{in}}$ after Δt.

The applied calculation scheme is robust, but gives only acceptable results when the changes ΔC during a time step are not too large. In ERSEM we make use of an adaptive time-step algorithm that min-

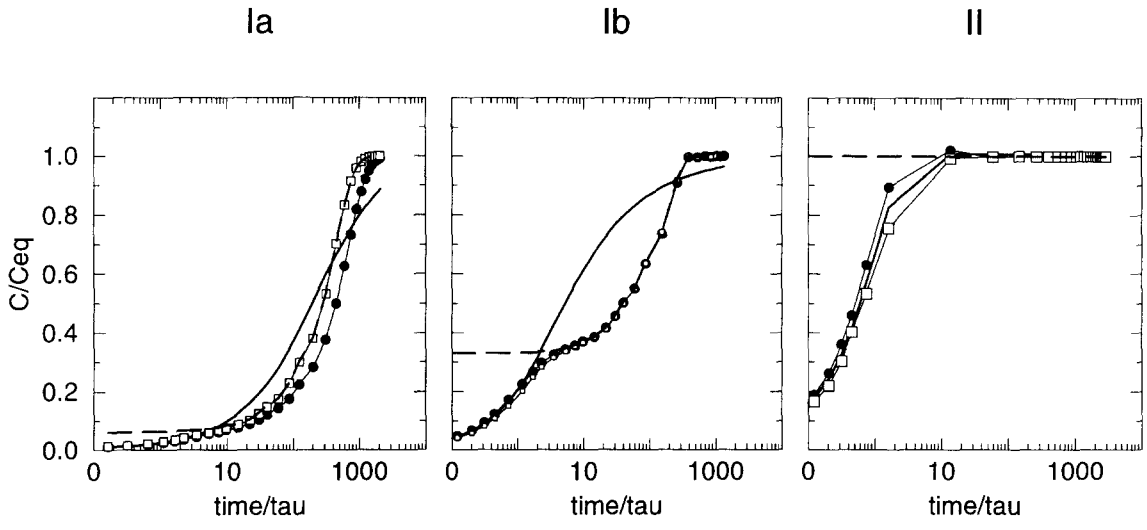

Fig. 5. The change in time of $\overline{C}$ modelled (line with squares), $\overline{C_{eq}}$ (broken line), $\overline{C_{tr}}$ (line with points) and $\overline{C}$ calculated with the analytical solution (solid line) for the same cases as described in caption of the previous figure. The circles and squares refer to the points in time at which the fluxes are calculated during the simulation. The step size is controlled by the condition that $\Delta C \cdot \Delta t/\overline{C} < 0.5$. On the Y-axis the actual concentration is divided by the average concentration of $\overline{C_\infty}$, the concentration for the case that the whole gradient ($0 < z < \infty$) is in equilibrium.

imizes the step sizes at large values of ΔC. Thus the length of a time-step is inversely proportional to the largest derivative ΔC occurring in the model. This together with the 'steady-state and correction' scheme prevents any instability of the model solutions.

To test the applicability of the calculation method we defined three hypothetical situations for which exact solutions of the dynamical Eq. 2 could be found in Carslaw & Jaeger (1946). For these solutions see Appendix B. In a two-layer sediment we assumed:

Ia. Constant 0-order M in both layers. No first-order process ($k = 0$).
Ib. As Ia, but $M = 0$ in the lower layer.
II. Constant 0-order M, but also a first-order reaction in the upper layer.

For boundary and initial conditions see caption of Fig. 4.

Resulting profiles after the first time step are shown in Fig. 4. Even under such a rigorous change of conditions, the model calculated the right average concentrations in the layers. The fluxes across the sediment-water interface are calculated from the gradients of the transient profiles, and these deviate slightly from the analytically derived gradients at $z = 0$. The dynamics of both the average concentration $\overline{C}$ and the sediment-water fluxes thus seem adequately modelled (Fig. 5). During normal simulations runs, dramatic changes as in the hypothetical test cases do not occur and we expect the model to perform even better than demonstrated in Figs 4 and 5. We conclude that small errors in fluxes and concentrations may be generated by the numerical scheme only for short periods, *e.g.* directly after mass deposition of organic matter at the sea floor. Generally the method works adequately and we believe that it is sufficiently accurate for our purpose.

4. THE SUBMODULES

4.1. GENERAL

Below we describe the submodules for ammonium, nitrate, phosphate and silica. The interrelations between the different submodules are given in Fig. 6. As mentioned in the introduction, the sediment is divided into maximally three functional layers (oxic layer, denitrification layer and sulphide layer). The depths of the interfaces between these layers are dynamically modelled and are coupled to the diagenetic redox processes. The upper interface is the oxygen penetration depth (z_{ox}). The second interface, the sulphide horizon (z_{an}) is the depth at which sulphate reduction becomes dominant. In between these surfaces nitrate is assumed to be the main oxidant. Manganese and iron are assumed to occur in their oxidized forms in the upper two layers and in their reduced forms below the second interface. Particularly the reduc-

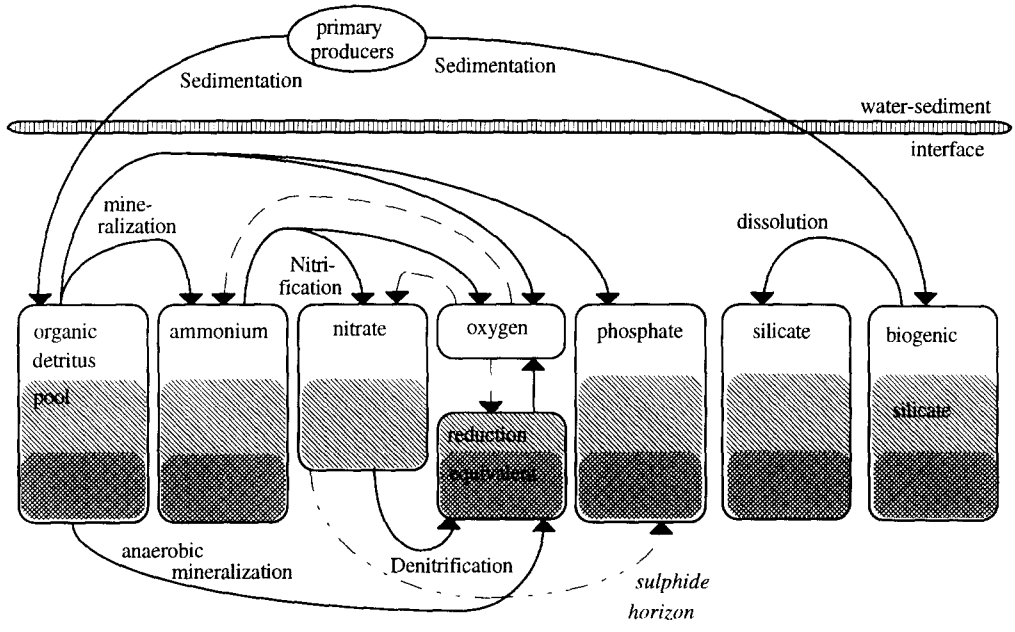

Fig. 6. The interrelations (arrows) between the different submodules. The input to the benthic system is controlled by the settling of remains of phytoplankton. This input arrives in the benthic organic pool (particulate carbon including N and P) or in the biogenic silica pool. The main driving and controlling force of the benthic nutrient processes is mineralization: phosphate, ammonium, oxygen and reduction equivalents are directly affected. Nitrate is coupled to mineralization through nitrification. The oxygen consumption by mineralization, nitrification and oxidation of reduction equivalents determines the interstitial oxygen concentration and the oxygen penetration depth. The oxygen penetration (dashed lines) modifies the nutrient dynamics considerably. The sulphide horizon depth (dotted-dotted line), derived from the nitrate module controls the adsorption properties of phosphate. Silicate is the only nutrient which is not affected by one of the other variables.

tion of Fe(III) to Fe(II) is important to describe different sorption properties of phosphate in the upper two and in the lower layers. The reduction of electron acceptors and the production of ammonium and phosphate are related to the decomposition of organic matter. Decomposition rates are obtained from the benthic biology module of ERSEM (Ebenhöh *et al.*, 1995). Other variables directly related to the activity of benthic organisms, such as bioirrigation and bioturbation, are also calculated as in this benthic biology module. Burial of organic matter and nutrients in the North Sea mainly occurs in the Skagerrak (Eisma, 1987) outside the area covered by ERSEM, and for this reason is not incorporated in the present modules.

4.2. AMMONIUM

Mineralization is the main process controlling ammonium dynamics. Other processes are nitrification, adsorption and of course vertical transport. We apply the steady state model described by Van Raaphorst *et al.* (1990), which in turn is a modification of the models of Vanderborght & Billen (1975) and Vanderborght *et al.* (1977a). In their nitrate models Goloway & Bender (1982) and Jahnke *et al.* (1982) assumed that ammonium released during oxidation of organic matter is immediately converted into nitrate when sufficient oxygen is present, without any build-up of reaction intermediates. When describing both nitrate and ammonium, such a rapid conversion is best formulated as a first-order nitrification rate. This approach is further justified by the expected ammonium concentrations in the oxic few upper mm of the sediment in most of the ERSEM boxes (< 25 mmol $N \cdot m^{-3}$), which are low compared to the half saturation constant for ammonium oxidation (Henriksen & Kemp, 1988). The adsorption of ammonium onto sediment particles by ion exchange reactions is considered a fast process and consequently the ammonium distribution between the solvent (pore water) and the sorbent phase (sediment particles) is assumed to be in equilibrium. The equilibrium distribution is mostly characterized by a linear distribution coefficient (Mackin & Aller, 1984) and is implemented in the model as a reduction of the apparent rate parameters (*e.g.* mineralization, nitrification and diffusion) (Berner, 1976). Following Vander-

TEXTBOX 1 *Set of equations in the ammonium and nitrate model*

$$(p+1)\frac{\partial A(z)}{\partial t} = D_A \frac{\partial^2 A(z)}{\partial z^2} - kA(z) + M_A \qquad (0 \le z \le z_{ox})$$

$$\frac{\partial N(z)}{\partial t} = D_N \frac{\partial^2 N(z)}{\partial z^2} + kA(z) \qquad (0 \le z \le z_{ox})$$

$$(p+1)\frac{\partial A(z)}{\partial t} = D_A \frac{\partial^2 A(z)}{\partial z^2} + M_A e^{-\alpha\zeta} \qquad (z > z_{ox})$$

$$\frac{\partial N(z)}{\partial t} = D_N \frac{\partial^2 N(z)}{\partial z^2} - d_N N(z) \qquad (z > z_{ox})$$

where:

$A(z)$: ammonium concentration in the pore-water (mmol N·m^{-3}).
$N(z)$: nitrate concentration in the pore-water (mmol N·m^{-3}).
z_{ox}: oxygen penetration depth (m).
$\zeta = z - z_{ox}$ (m).
D_A: whole sediment diffusion constant of ammonium (m^2·d^{-1}).
D_N: whole sediment diffusion constant of nitrate (m^2·d^{-1}).
k: specific nitrification rate (d^{-1}).
d_N: specific denitrification rate (d^{-1}).
M_A: ammonium production through mineralization in the oxic layer (mmol N·m^{-3}·d^{-1}).
α: constant, describing the exponential decrease of mineralization with depth (m^{-1}).
p: adsorption distribution coefficient of ammonium (-).

The equations for each nutrient are linked by stating continuity in the concentration and the flux at $z = z_{ox}$. The boundary conditions are for $z = 0$: $A = A(0)$ and $N = N(0)$ and for $z \to \infty$: $\partial A/\partial z = 0$ and $N(z) \to 0$.

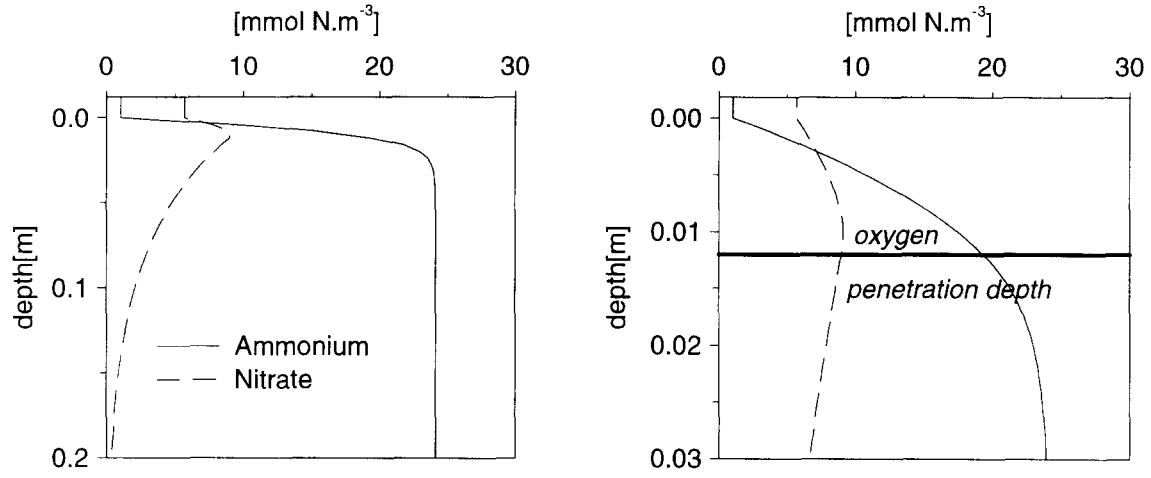

Fig. 7. Steady-state profiles for ammonium and nitrate in the upper 20 cm and upper 3 cm of the sediment obtained from the equations listed in textbox 1.

borght & Billen (1975) the sediments are partitioned in two layers: a nitrification zone extending from $z = 0$ at the sediment surface to the oxygen penetration depth (z_{ox}), and a zone below where nitrification is absent. The ammonium production is described by a zero-order reaction in the upper layer and with a declining exponential term in the lower layer. The set of partial differential equations for ammonium is given in textbox 1. In Fig. 7 an example of a steady-state ammonium profile is given.

4.3. NITRATE

Nitrate is coupled to ammonium through nitrification in the oxic layer. Denitrification is described as a first-order loss process. Steady state models to describe nitrification and denitrification including vertical transports are well-established (Vanderborght & Billen, 1975; Vanderborght *et al.*, 1977a; Van Raaphorst *et al.*, 1990).

The general set of partial differential equations is

TEXTBOX 2 *Set of partial differential equations applied for phosphate.*

$$(p_{ox}+1)\frac{\partial P(z)}{\partial t} = D_P \frac{\partial^2 P(z)}{\partial z^2} + M_P \qquad (0 \le z \le z_{ox})$$

$$(p_{ox}+1)\frac{\partial P(z)}{\partial t} = D_P \frac{\partial^2 P(z)}{\partial z^2} + M_P e^{-\alpha\zeta} \qquad (z_{ox} < z \le z_{an})$$

$$(p_{an}+1)\frac{\partial P(z)}{\partial t} = D_P \frac{\partial^2 P(z)}{\partial z^2} + M_P e^{-\alpha\zeta} \qquad (z > z_{an})$$

In these equations:

$P(z)$: phosphate concentration in the pore water (mmol P·m^{-3} pw).

z_{ox}: oxygen penetration depth (m).

z_{an}: sulphide horizon (m).

$\zeta = z - z_{ox}$ (m).

D_P: whole sediment diffusion constant for phosphate (m^2·d^{-1}).

M_P: phosphate production through mineralization in the oxic layer (mmol P·m^{-3}·d^{-1}).

α: constant, describing the exponential decrease of mineralization with depth (m^{-1}).

p_{ox}: adsorption distribution coefficient of phosphate in the oxic and denitrification layer (-).

p_{an}: adsorption distribution coefficient of phosphate in the sulphide layer (-).

The three equations are linked by stating continuity in the concentration and the flux at the interfaces between the 3 layers. The boundary conditions are $z = 0 : P = P(0)$ and $z \to \infty$: $\partial P(z)/\partial z \to 0$.

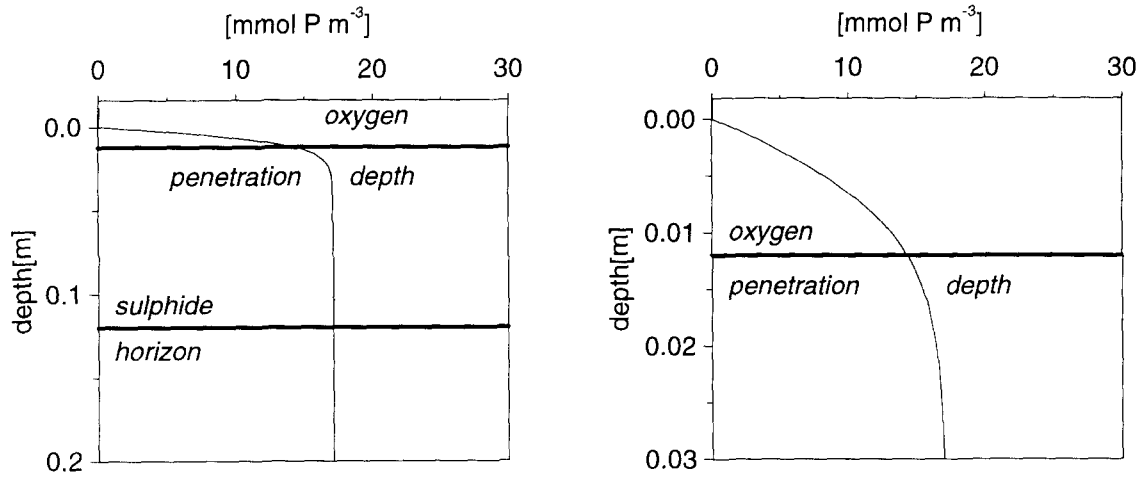

Fig. 8. The steady-state profiles for phosphate in upper 20 cm and upper 3 cm of the sediment.

given in textbox 1. Fig. 7 gives an example of a steady-state nitrate profile obtained with this set of equations.

4.4. PHOSPHATE

Adsorption is an important process in sedimentary phosphate dynamics (Van Raaphorst *et al.*, 1988; Sundby *et al.*, 1992). It is assumed that reduction of Fe(III) concurrently mobilizes Fe(II) and adsorbed phosphate in the sulphide layer. We expect that the nitrate concentration remains sufficiently high in the denitrification layer to inhibit the reduction of Fe(III). Thus it is assumed that the proportion between adsorbed and dissolved phosphate is considerably less (2:1, Krom & Berner, 1980) in the sulphide layer than in the upper two layers (250 to 400:1, see section 5.). Sorption of phosphate is considered as a fast process and consequently the phosphate concentration in the solvent phase (pore-water) and the sorbent phase (sediment particles) are in equilibrium. The phosphate production in the oxic layer is described as a zero-order reaction declining exponentially below $z = z_{ox}$ and is stoichiometrically coupled to the carbon and ammonium mineralization. The set of equations ap-

TEXTBOX 3 *Set of partial differential equations applied for silicate.*

$$\frac{\partial C(z)}{\partial t} = D_{Si}\frac{\partial^2 C(z)}{\partial z^2} - dB_1 \qquad (0 \le z \le z_{ox})$$

$$\frac{\partial C(z)}{\partial t} = D_{Si}\frac{\partial^2 C(z)}{\partial z^2} - \frac{sB_1 e^{-\beta\zeta}}{Si_\infty}C(z) \qquad (z > z_{ox})$$

where:

$C(z)$= $Si_\infty - Si(z)$ (mmol Si·m^{-3}).

Si_∞: concentration of dissolved silica at saturation with opaline silica (mmol Si·m^{-3}).

$Si(z)$: concentration of dissolved silica (mmol Si·m^{-3}).

z_{ox}: oxygen penetration depth (m).

ζ = $z - z_{ox}$ (m).

D_{Si}: whole sediment diffusion constant (m^2·d^{-1}).

β: parameter that describes the negative exponential decline of B (m^{-1}).

s: first-order dissolution constant of biogenic silica (d^{-1}).

B_1: average concentration of biogenic silica in the oxic layer (mmol Si·m^{-3}).

The two equations are linked by stating continuity in the concentration and the flux $z = z_{ox}$. The boundary conditions are $z = 0$: $C = Si_\infty - Si(0)$ and $z \to \infty$ $\partial Si/\partial x \to 0$.

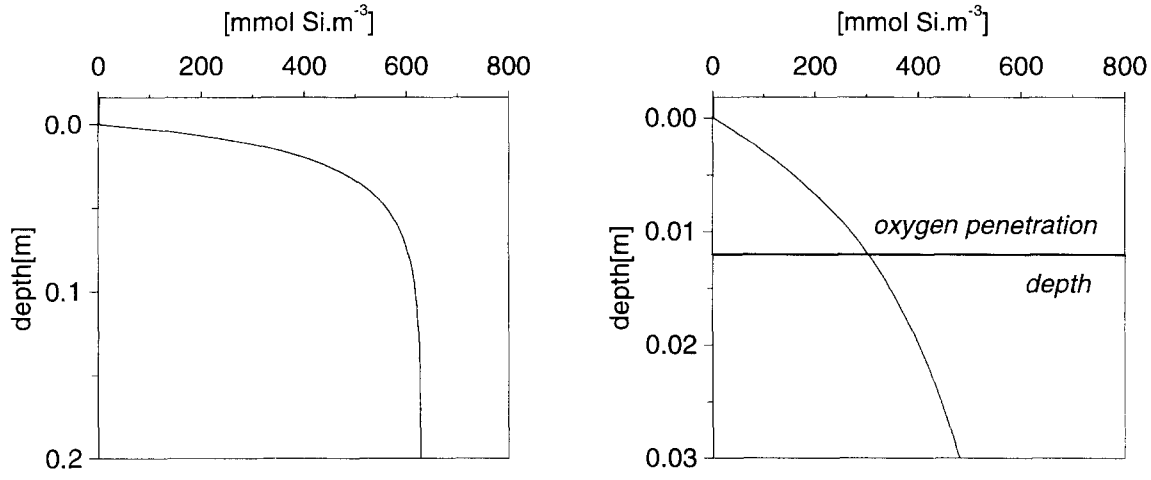

Fig. 9. The steady-state profiles for silicate in the upper 20 cm and upper 3 cm of the sediment.

plied in the phosphate submodels is presented in textbox 2. An example of steady state phosphate profiles obtained with this set of equations is given in Fig. 8.

4.5. SILICA

Diatoms have skeletons consisting of opaline silica. Once they die, their siliceous frustiles settle to the sediment and undergo dissolution. This submodel describes the processes affecting biogenic silica after deposition on the sea floor: dissolution to dissolved silica and the vertical transports. The transport of particulate biogenic silica is modelled analogously to the particulate carbon transport in the sediment (Ebenhöh *et al.*, 1995).

The dissolution of biogenic silica is described as a first-order process in both biogenic silica and dissolved silica (Hurd, 1973; Schink *et al.*, 1975):

$$R_d = \frac{sB}{Si_\infty}(Si_\infty - Si) \qquad (5)$$

where

R_d: dissolution rate of biogenic silica (mmol Si·m^{-3}·d^{-1}).

s: first-order dissolution constant of biogenic silica (d^{-1}).

B: concentration of biogenic silica (mmol Si·m^{-3}).

Si: concentration of dissolved silica(mmol Si·m^{-3}).

Si_∞: concentration of dissolved silica at saturation with opaline silica (mmol Si·m^{-3}).

Schink *et al.* (1975) considered only the reactive or easily soluble part of the biogenic silica, other

forms of solid silica such as clays and quartz were neglected:

$$\frac{\partial Si(z)}{\partial t} = D_{Si}\frac{\partial^2 Si(z)}{\partial z^2} + sB(z)\frac{Si_\infty - Si(z)}{Si_\infty} \quad (6)$$

in which D_{Si} is the apparent whole sediment diffusion constant for silica. In general, solving of Eq. 6 can be done only by numerical methods, which as pointed out in the Introduction is not desirable in an ecosystem model such as ERSEM. Therefore we simplified Eq. 6. The first simplification is that at low pore-water concentrations in the oxic zone ($z < z_{ox}$) of the sediment the first-order dissolution essentially behaves as a zero-order reaction:

$$sB(z)\frac{Si_\infty - Si(z)}{Si_\infty} \approx s\overline{B_1} \qquad (0 < z \leq z_{ox}) \quad (7)$$

where $\overline{B_1}$ is the average concentration in the oxic layer. The most crucial simplification is that we approximate the gradient of the biogenic silica below the oxygen penetration depth by an exponential function:

$$sB(z)\frac{Si_\infty - Si(z)}{Si_\infty} \approx sB_1 \cdot e^{-\beta z}\frac{Si_\infty - Si(z)}{Si_\infty} \qquad (z \geq z_{ox}) \quad (8)$$

in which β (m^{-1}) is the parameter describing the exponential decline of the biogenic silica contents. The simplification is supported by the profiles of reactive particulate silica measured by Gehlen & Van Raaphorst (1993) in sandy North Sea sediments. The resulting set of equations are listed in textbox 3. The solution for the differential equations consists of Bessel functions that may be obtained with standard numerical techniques (Abramowitz & Stegun, 1964; Press *et al.*, 1986) (see Appendix C.). Examples of the resulting steady-state profiles are given in Fig. 9.

4.6. REDUCTION EQUIVALENTS

In the North Sea the oxygen penetration in sediments varies from a few mm in coastal to a few cm in offshore areas (Lohse *et al.*, 1993). Nitrate may penetrate much deeper than oxygen (Jørgensen, 1989; Van Raaphorst *et al.*, 1990). In the reduced sediment below, sulphate reduction is mostly the dominant process in the degradation of organic matter (Froelich *et al.*, 1979). Modelling of the anaerobic oxidation reactions is important for two reasons. First, it is necessary to maintain mass conservation. Second, ions reduced by anaerobic mineralization can substantially add to oxygen demands in the oxic sediment layer and thus influence the oxygen penetration depth (Billen, 1982). Oxidation of reduced components as Fe(II), Mn(II) or HS^- may even dominate oxygen consumption rates at specific locations during certain periods in the seasonal cycle (Canfield *et al.*, 1993). Modelling of all the redox elements explicitly is not necessary, however, for our purpose. Instead we introduce only one state variable representing all reduced ions generated in the sulphide layer. We define these ions as reduction equivalents, and assume that they have the properties of sulphide (*e.g.* diffusion coefficient). The reduction equivalents diffuse upward towards the oxic layer where they are oxidized by O_2. We assume that they are not oxidized by NO_3^-. The oxidation rate M_r is determined from the additional boundary condition $\frac{\partial R}{\partial z} = 0$ at $z = 0$. The general set of partial differential equations applied to reduction equivalents is given in textbox 4. Examples of steady-state profiles obtained with this set of equations are given in Fig. 10.

4.7. OXYGEN PENETRATION DEPTH AND SULPHIDE HORIZON

The oxygen penetration depth (z_{ox}) and the depth at which the sulphate reduction starts (z_{an}) have to be known before the nutrient equations can be solved. Mineralization of organic matter is the main O_2-consuming process, but nitrification and oxidation of reduced ions can enhance the O_2 consumption considerably. We apply the model of Bouldin (1968) to calculate the O_2 profiles and penetration depths (textbox 5). In contrast to Bouldin (1968), however, we included zero-order consumption rates to take nitrification and oxidation of reduction equivalents into account. The interface between the denitrification layer and the sulphide layer (z_{an}), called the sulphide horizon, is derived from the nitrate submodel. The nitrate gradient shows an exponential decrease with depth due to denitrification below z_{ox} (Fig. 7). Following the criterion of Van Raaphorst *et al.* (1990) we defined the sulphide horizon (z_{an}) as the depth at which denitrification has decreased to 10% of its initial value at the oxygen penetration depth (textbox 5).

5. PARAMETERS

5.1. EXTERNAL PARAMETERS

The parameters are divided in two groups. The first group consists of parameters which are calculated outside the nutrient submodels and from there are introduced into the benthic nutrient submodels (Table 1). All mineralization rates are within this group of ex-

TEXTBOX 4 *Set of partial differential equations applied for reduction equivalents.*

$$\frac{\partial R(z)}{\partial t} = D_S \frac{\partial^2 R(z)}{\partial z^2} - M_r \qquad (0 \leq z \leq z_{ox})$$

$$\frac{\partial R(z)}{\partial t} = D_S \frac{\partial^2 R(z)}{\partial z^2} + \frac{M_o}{\eta_r} e^{-\alpha\zeta} - \xi_d d N(z) \qquad (z > z_{ox})$$

In these equations:

$R(z)$: reduction equivalent concentration in the pore-water (mmol S·m^{-3}).

$N(z)$: nitrate concentration in the pore water(mmol N·m^{-3}).

z_{ox}: oxygen penetration depth (m).

$\zeta = z - z_{ox}$ (m).

D_S: diffusion coefficient of sulphide (m^2·d^{-1}).

M_o: formation of reduction equivalents through anoxic carbon mineralization (mmol O_2·m^{-3}·d^{-1}).

η_r: O_2 :S^{2-}conversion factor (=2 mmol O_2·(mmol S^{2-})$^{-1}$).

α: constant, describing the exponential decrease of mineralization with depth (m^{-1}).

M_r: zero-order coefficient describing the oxidation of reduction equivalents by O_2 (mmol S^{2-}·m^{-3}·d^{-1}).

d: first-order denitrification rate for oxidation of organic carbon by nitrate (d^{-1}).

ξ_d: denitrification stoichiometric factor (= 0.625 mmol S· (mmol N)$^{-1}$).

M_r is unknown and calculated from the steady-state solution. The two equations are linked by stating continuity in the concentration and the flux at $z = z_{ox}$. The boundary conditions are $z = 0$: $R = 0$ and $\partial R/\partial z = 0$ and $z \to \infty$: $\partial R/\partial z \to 0$.

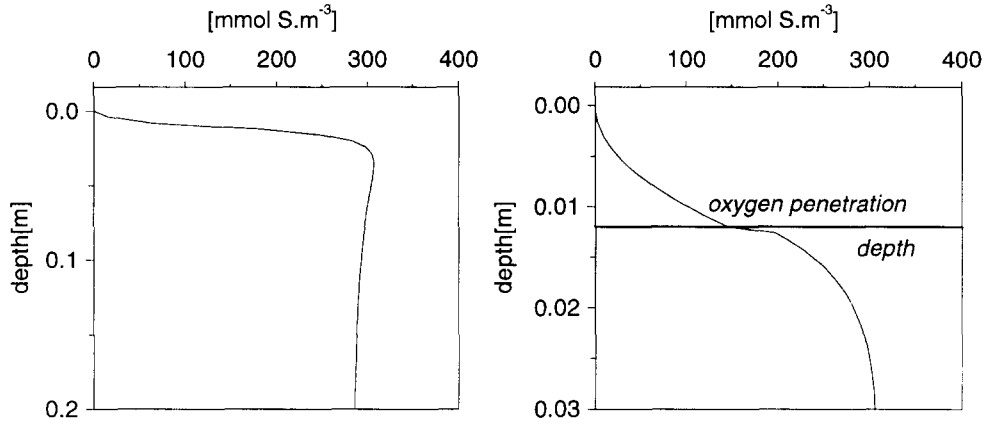

Fig. 10. Steady-state profile for reduction equivalents in the upper 20 cm and upper 3 cm of the sediment.

ternal parameters. The second group of parameters is specified in the benthic nutrient submodels. These parameters may be corrected for temperature, bioirrigation and porosity of the sediments. The latter three variables are either taken as forcing functions from outside the ERSEM model, or are calculated in the benthic biology model (Ebenhöh *et al.*, 1995).

The main source of organic matter to the benthic system is detritus, generated in the pelagic system and deposited on the sea floor or filtered by suspension feeders. Subsequently the detritus is redistributed in the sediment by particulate transport and bioturbation and decomposed by benthic organisms. All these processes are described in the benthic biology model. In our model it is assumed that the detritus is exponentially distributed with depth. The steepness of this exponential distribution is recalculated from the output of the benthic biology model. The decomposition of organic matter in the benthic biology model is effectuated by bacteria and macrobenthos which consume detritus for their growth. In the benthic biology model it is assumed that all benthic organisms live in the oxic layer. For the thickness of this layer the value of z_{ox} from the previous time step is used. The total mineralization in the oxic layer is derived from the sum of all respirations (O_2) and all excretions (N and P) of the benthic organisms in this layer. In the other layers the mineralization is caused by the activity of anaerobic bacteria. These mineralizations are the main input to the benthic nutrient model. The parameter α is

TEXTBOX 5 *Set of partial differential equations for oxygen.*

$$0 = D_{Ox}\frac{\partial^2 Ox(z)}{\partial z^2} - M - \eta_r M_r - M_n \qquad (0 \le z \le z_{ox})$$

$$z_{ox} = \sqrt{\frac{2DOx_0}{M + \eta_r M_o + M_n}}$$

$$z_{an} = \log 0.10/\sqrt{d/D_N} + z_{ox}$$

in which:

Ox: O_2 (mmol O_2·m^{-3}).
z_{ox}: O_2 penetration depth (m).
z_{an}: sulphide horizon (m).
D_{Ox}: diffusion constant of oxygen (m^2·d^{-1}).
D_N: diffusion constant of nitrate (m^2·d^{-1}).
M: zero-order O_2 consumption rate (mmol O_2·m^{-3}·d^{-1}).
M_r: zero-order oxidation rate of reduction equivalents (mmol S^{2-}·m^{-3}·d^{-1}).
η_r: O_2:S^{2-}conversion factor (=2 (mmol O_2)·(mmol S)$^{-1}$).
d: denitrification constant (d^{-1}).
M_n: average nitrification rate (mmol O_2·m^{-3}·d^{-1}). Defined as:

$$M_n = \frac{\xi_k k}{z_{ox}} \int_{z=0}^{z_{ox}} A(z)dz$$

k: nitrification constant (d^{-1}).
ξ_k: nitrification stoichiometric factor (= 2 mmol O_2·(mmol N)$^{-1}$).
$A(z)$: NH_4^+ concentration (mmol N·m^{-3}).

The boundary conditions for the equation are $z = 0$: $Ox = Ox(0)$ and $z \ge z_{ox}$: $Ox(z) = 0$.

TABLE 1.
Overview of the input variables into the benthic nutrient model.

variable	*variable type*	*calculated in submodel*
P-mineralization	rate	benthic biology model
N-mineralization	rate	benthic biology model
O_2-mineralization	rate	benthic biology model
distribution biogenic silica	environmental variable	benthic biology model
temperature	forcing function	
bioirrigation	environmental variable	benthic biology model
porosity	environmental variable	parameter

calculated from the difference between the oxic and anoxic mineralizations (see textboxes 1, 2 and 4):

$$M = \frac{\overline{\mathcal{M}}}{\alpha \cdot H}(1 - e^{-\alpha H}) \qquad (9)$$

where M is the average mineralization in the oxic layer (mmol·m^{-3}·d^{-1}), $\overline{\mathcal{M}}$ is the depth-averaged mineralization in the layers below $z = z_{ox}$ (mmol·m^{-3}·d^{-1}) and H (=0.3−z_{ox}) is the thickness of the two lower layers (m).

The vertical transport of particulate biogenic silica is modelled in a similar way as C, N and P. This is also done in the benthic biology model. 'Decomposition' of silica (=dissolution) is fully described in the nutrient submodel (section 4.5.).

The physical characteristics of the sediments in the ERSEM boxes are an important factor for the diagenetic processes in the sediments. Sedimentary contents of organic matter and other reactive components as *e.g.* Fe are often correlated with grain size distribution and porosity (Mackin & Aller, 1984; Wiesner *et al.*, 1990). Basford & Eleftheriou (1988) found a general decrease in the median particle size of sediments going from west to east in the northern North Sea. Wiesner *et al.* (1990) gave a detailed review of grain size distribution and porosities in the German Bight area. The estimation of the average porosity in the boxes in the northern part (1/11, 2/12, 3/13, 4/14 and 6) is done by combining a relation between porosity and median particle size (see Fig. 12a), and observations of Basford & Eleftheriou (1988) and Wiesner *et al.* (1990). For the estimation of the average porosity parameter values for the boxes in the southern part of the North Sea (box 5/15, 7, 8, 9 and 10) recent observations by Lohse *et al.* (1993) were used.

5.2. INTERNAL PARAMETERS

Diffusion Molecular diffusion coefficients were obtained from Li & Gregory (1974) (Table 2). The diffusion coefficient is corrected for temperature (correction factor: C_T), bioirrigation (C_B) and tortuousity (C_p) according to:

$$D = D_m \cdot C_T \cdot C_B \cdot C_p \qquad (10)$$

Temperature correction is based on the Stokes-Einstein relation as described in Li & Gregory (1974). Only the molecular diffusion coefficient of oxygen was calculated from an equation fitting to data of Broecker & Peng (1973) and Himmelblau (1964) in which already a temperature (T, °C) correction is included:

$$D_O = 10^{-9} \cdot 10^{3.672 - \frac{984.26}{273+T}} \quad (\mathrm{m^2 \cdot sec^{-1}}) \qquad (11)$$

Bioirrigation is calculated in the benthic biology module (Ebenhöh *et al.*, 1995) and depends mainly on activity and biomass of macrobenthos. The diffusion is corrected for the tortuousity using the relation of Ullman & Aller (1982) for ϕ <0.7 ($C_p = 1$).

Nitrogen Nitrification and denitrification are modelled as first-order loss processes of ammonium and nitrate, respectively. For both processes specific rates at 10 °C are defined as parameters and are corrected for the ambient temperature assuming a Q10 of 2. In sediments with low nitrate concentrations in the overlying water a close coupling between nitrification and denitrification can be found (Jenkins & Kemp, 1984; Van Raaphorst *et al.*, 1990). Values of the first-order constants of both processes derived from pore-water profiles are often correlated to each other (Jahnke *et al.*, 1982). Consequently these values cannot be estimated independently. First-order nitrification rate constants are not often reported in the literature. We therefore took the denitrification rate from literature and estimated the nitrification constant by calibration of the model. Values of the denitrification rate constant reported in the literature vary over a few order of magnitude from 10^{-10} to 10^{-2} d^{-1} in oceanic sediments (Jahnke *et al.*, 1982; Goloway & Bender, 1982) to 0.1 to 20 d^{-1} in muddy coastal sediments. (Billen, 1978; Aller *et al.*, 1985). We applied a value of 0.17 d^{-1} to account for the largely sandy sediments in the North Sea. This value is less than the relatively high rates obtained by Van Raaphorst *et al.* (1990) for the Dogger Bank area. Nitrification was calibrated by comparing model outputs with the empirical relation between denitrification and nitrification as summarized by Van Raaphorst *et al.* (1990) for marine sediments (Fig. 11). With a first-order nitrification rate of 1.5 d^{-1} at 10 °C we obtained nitrification and denitrification rates close to this empirical relation. According to Mackin & Aller (1984) the distribution coefficient for ammonium adsorption (p, see textbox 2) is relatively invariable between 1.0 and 1.7. Recent data do indicate, however, that much higher values can occur, particularly in the upper layers of the sediment with low NH_4^+ concentrations. Based on the values of Laima (1992) and Malschaert & Van Raaphorst (1993) we estimated p for ammonium at 3.

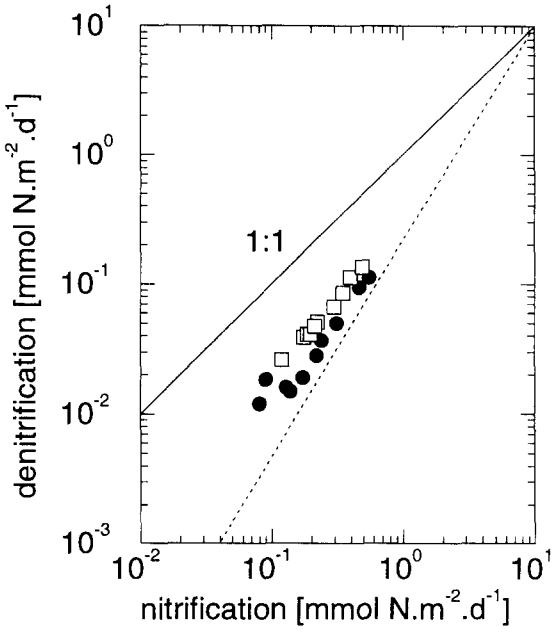

Fig. 11. Relation between whole sediment nitrification and denitrification as summarized by Van Raaphorst *et al.* (1990) (dotted line) and results of the calibration run. The points represent the relation between the monthly averaged values of nitrification and denitrification fluxes for the months February (□) and August (•).

Phosphate Slomp & Van Raaphorst (1993b) found a positive linear relationship between porosity and the adsorption coefficient of phosphate K_a (Fig. 12). The adsorption distribution coefficient, applied in the model is derived from K_a according to:

$$p = K_a \frac{1-\phi}{\phi} \rho$$

In which ρ is the density of sediment particles ($g \cdot m^{-3}$). The values derived from this equation, using

TABLE 2.
Overview of the basic parameters.

basic parameter		*value*	*literature reference*
adsorption (-)	phosphate	box dependent	see Table 3
	ammonium	3.0	Laima (1992)
			Malschaert & Van Raaphorst (1993)
molecular diffusion	phosphate	$64.8 \cdot 10^{-6}$	Li & Gregory (1974)
coefficient at 25 °C	ammonium	$173.0 \cdot 10^{-6}$	Li & Gregory (1974)
($m^2 d^{-1}$)	nitrate	$164.0 \cdot 10^{-6}$	Li & Gregory (1974)
	silicate	$35.0 \cdot 10^{-6}$	Li & Gregory (1974)
	reduction equivalents	$35.0 \cdot 10^{-6}$	Li & Gregory (1974)
	oxygen	—	see text
Q_{10}	biological processes	2.0	
specific nitrification rate (d^{-1})		1.5	calibrated
specific denitrification rate (d^{-1})		0.17	Van Raaphorst *et al.* (1990)
specific dissolution rate of silica (d^{-1})		0.17	calibrated
equilibrium concentration		temperature	see further text
of silica(Si_∞, mmol Si·m^{-3})		dependent	

TABLE 3.
Overview of the box-dependent parameters.

box nummer	*porosity*	*phosphate adsorption distribution coefficient*
1/11	0.60	400
2/12	0.50	400
3/13	0.70	400
4/14	0.50	400
5/15	0.50	250
6	0.40	100
7	0.40	100
8	0.40	50
9	0.50	400
10	0.40	100

the North Sea porosity data and the relation in Fig. 12 are given in Table 3.

Silica In the model dissolution of silica depends on two parameters: a first-order dissolution rate (s, textbox 3) and a parameter representing the concentration of dissolved silica at saturation with biogenic (opaline) silica (Si_∞). Vanderborght *et al.* (1977b) and Gehlen *et al.* (1993) report values of Si_∞ in the range from 400 to 600 mmol Si·m^{-3} obtained from porewater profiles and dissolution experiments of sandy North Sea sediments. In deposition areas as the inner German Bight porewater concentrations more close to the dissolution equilibrium of opaline silica ($\approx$ 1000 mmol Si·m^{-3}; Hurd, 1973) are found (Gehlen & Van Raaphorst, unpublished data). Fanning & Pilson (1971) showed that the temperature at which the interstitial water was squeezed from a marine sediment had a profound effect on the measured interstitial silica concentration probably due to a change of Si_∞. Lawson *et al.* (1978) and Iler (1979) showed that the solubility of several Si-minerals increases with temperature. In accordance with these observations we apply a temperature dependent Si_∞ with values of about 400 mmol Si·m^{-3} in winter and of about 800 mmol Si·m^{-3} in summer:

$$Si_\infty = Si_{\infty,10} - a_T * (1 - 2^{(T-10)/10}) \quad (12)$$

in which:

$Si_{\infty,10}$: equilibrium concentration at 10 °C (= 600 mmol Si ·m^{-3})

a_T: amplitude of the equilibrium concentration (= 400 mmol Si ·m^{-3})

The first-order dissolution constant (s) is based on direct measurements of this constant reported in the literature. Values for North Sea sediments vary between 0.04 d^{-1} (Vanderborght *et al.*, 1977b) and 0.006 to 0.013 d^{-1} (Gehlen *et al.*, 1993). Based on these values we estimated the dissolution constant at 0.03 d^{-1}. This value is at the lower end of the range (0.025 to 0.36 d^{-1}) found by Van Raaphorst *et al.* (1990), who estimated these values indirectly from pore water profiles in the Dogger Bank area. Compared with values reported for Long Island Sound sediments (0.08 to 1.123 d^{-1}) (Aller, 1980)) we use a much lower value. For simplicity we used the same temperature dependency for the dissolution rate constant as for diffusion.

6. RESULTS

6.1. INPUT TO THE BENTHIC NUTRIENT MODEL

All results were obtained by running the full ERSEM model. The primary production (Fig. 13a), deposition

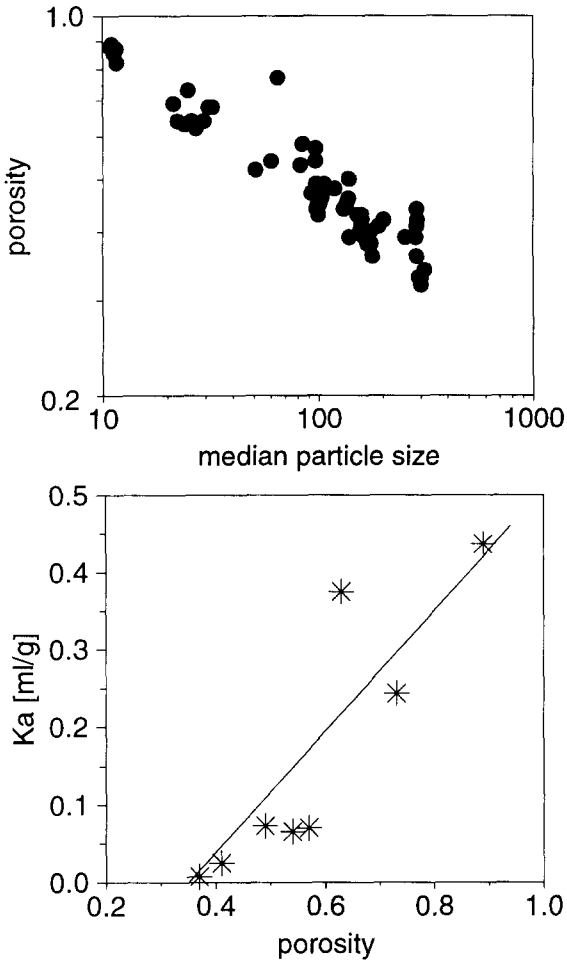

Fig. 12. a. Relation between median particulate size and the porosity of the sediment as measured in the North Sea (Van Raaphorst, unpublished data); b. Relation between adsorbed phosphate and the porosity of the sediment as measured in the North Sea (Slomp & Van Raaphorst, 1993b and Slomp, unpublished data).

of organic carbon (Figs 13b and 14) on the sediment and the coupled mineralization (Fig. 14) show distinct seasonal dynamics. Most of the sedimented material originates from local primary production. Estimation of primary production from ^{14}C-incubations yields a value somewhere between gross and net production (Peterson, 1980). Indeed, the primary production data of Joint & Pomroy (1993) are in between simulated net and gross production (Figs 13a and 13d). The resulting mineralization of particulate nutrients is used as input to the benthic nutrient model for the oxic layer and for the lower layers (Fig. 14). For N and P the benthic biology model calculates that the largest part of the mineralization takes place in the oxic layer. This is not only explained by the deposition of fresh detritus on top of the sediments. Also, the benthic fauna is assumed to feed in deeper layers and to excrete the excess of nutrients from the consumed detritus and bacteria in the oxic layer. Consequently, there is an upward transport of nutrients associated with the activity of the benthic fauna in the model. Silica dissolution occurs at a slower rate than mineralization of N and P, and is not affected by ingestion by benthic fauna distributed deeper into the sediment column.

The bioirrigation factor is estimated from the activity and the biomass of macrobenthos and shows highest values in late summer and lowest just before sedimentation of the spring bloom (Fig. 13c). For details refer to Ebenhöh *et al.* (1995). A remarkable result is that a large sedimentation (*e.g.* boxes 14 and 15) does not necessarily lead to a large bioirrigation (Fig. 13f). Fig. 13d shows that the lowest input of organic carbon to the sea floor is in the boxes 11 and 13.

6.2. PORE-WATER GRADIENTS AND FLUXES

Oxygen The model calculates benthic nutrient dynamics in ten different areas for a full annual cycle. To keep the number of results to be presented within reasonable limits, we will focus the discussion on the boxes 9 and 11. Box 9 represents the fully mixed coastal box in the German Bight with large nutrient inputs from the rivers. Box 11 is the lower box in the stratified part in the northern North Sea. Deposition of algal material directly after the spring bloom resulted in a short peak in the benthic oxygen consumption in box 9 (Fig. 15b). Similar peaks were calculated for the other shallow boxes (<30 m), but not for the boxes in the deeper parts of the North Sea (*e.g.* box 11). The maximum consumption rates were calculated from August (box 9) to October (box 11). These maxima are related to the deposition of detritus and to high temperatures during summer. Oxygen penetration depth is inversely coupled to the O_2 consumption and consequently shows an inverse seasonal pattern with the highest values just before the spring bloom and lowest in summer (Fig. 15a).

The proportion between aerobic and anoxic mineralization is controlled by the penetration depth of oxygen (Fig. 16a) and the total mineralization of organic matter. In box 9 oxygen consumption by nitrification is negligible, but 30-40% of the oxygen consumption during summer is used for oxidation of reduction equivalents diffusing upwards from the deeper layers (Fig. 15b). In the deeper box 11, nitrification forms a slightly more substantial part of the oxygen budget.

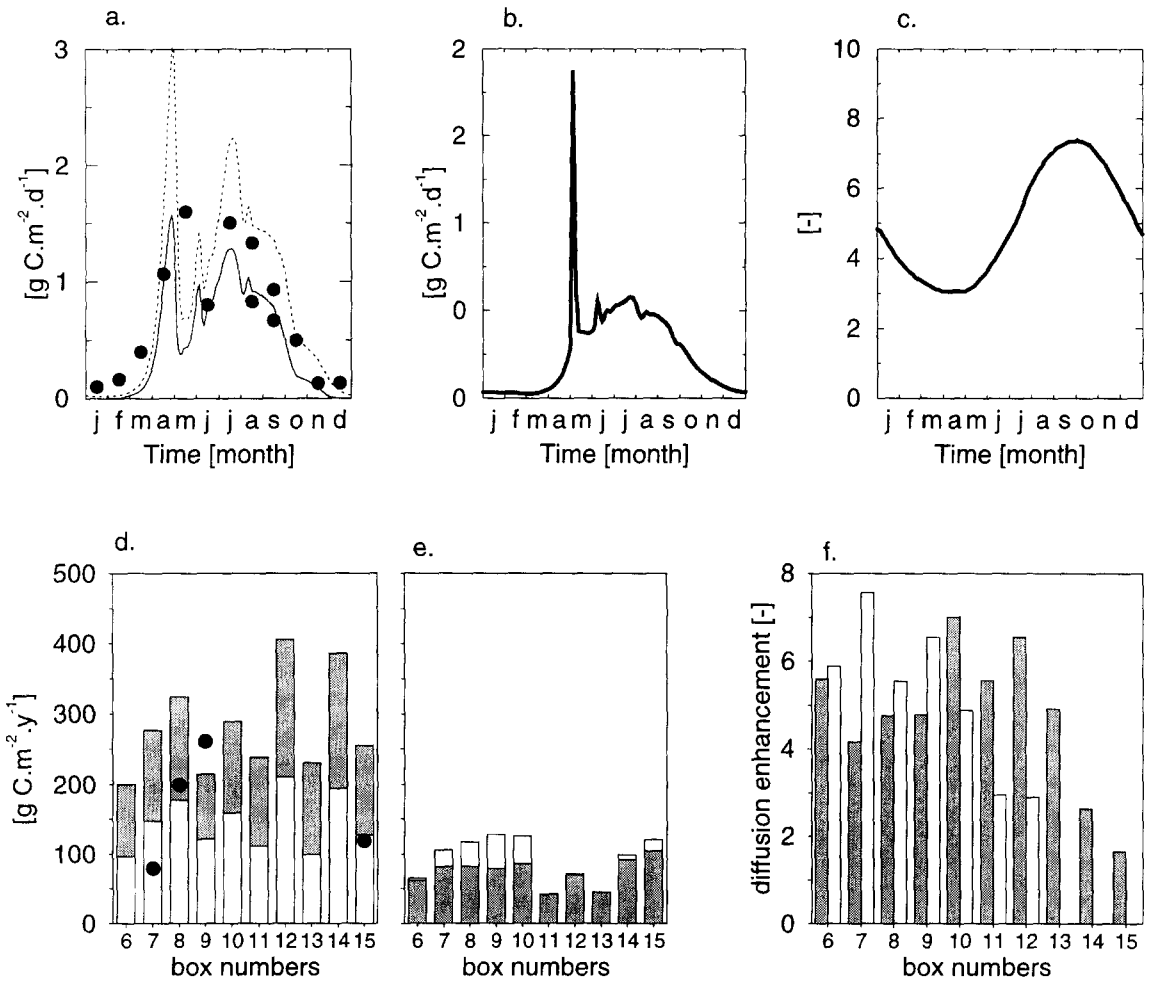

Fig. 13. a. The gross (solid line) and net (dotted line) primary production modelled with the ERSEM model for box 9 and field observations (•) of Joint & Pomroy (1993); b. The seasonal dynamics of deposition of organic material on the sea floor in box 9; c. Yearly variation of the bioirrigation factor C_B (Eq. 10) in box 9 as calculated by the benthic biology model (Ebenhöh *et al.*, 1995); d. Simulated annual gross (white + grey) and net (white) primary production based in the total water column above the sediment of the boxes and primary production based on field observations (•, Joint & Pomroy (1993)); e. Yearly input of organic carbon through sedimentation (grey) and through filtering of suspension feeders (white); f. Annual mean value of the bioirrigation C_B (grey) and of bioturbation factor (white). The latter value is given for completeness only and controls the vertical transport of particulate detritus and silica (Ebenhöh *et al.*, 1995).

Oxidation of reduction equivalents is less important in the boxes 11 and 13 than in the other boxes. In general the contribution of oxidation of reduction equivalents is most important in summer (Fig. 16c). Primary production in the deeper northern boxes (boxes 6, 11, 12 and 13) and the deposition of organic material onto the sediment is distinctly lower than in the other boxes (Fig. 13c). This is reflected in the total benthic oxygen consumption (Fig. 16b). The central boxes (14 and 15) have similar oxygen consumption rates as the adjacent coastal boxes with large river inputs (boxes 7, 8 and 9).

Ammonium and nitrate The ammonium profiles respond to changes in the ambient circumstances during the year (Fig. 17). The subsurface maxima of the calculated ammonium profiles of box 9 reflect steady-state conditions in summer and autumn due to the deposition of detrital material. The April profile just before the deposition of the spring bloom represents a situation with low ammonium production and depressed ammonium concentration in the oxic layer

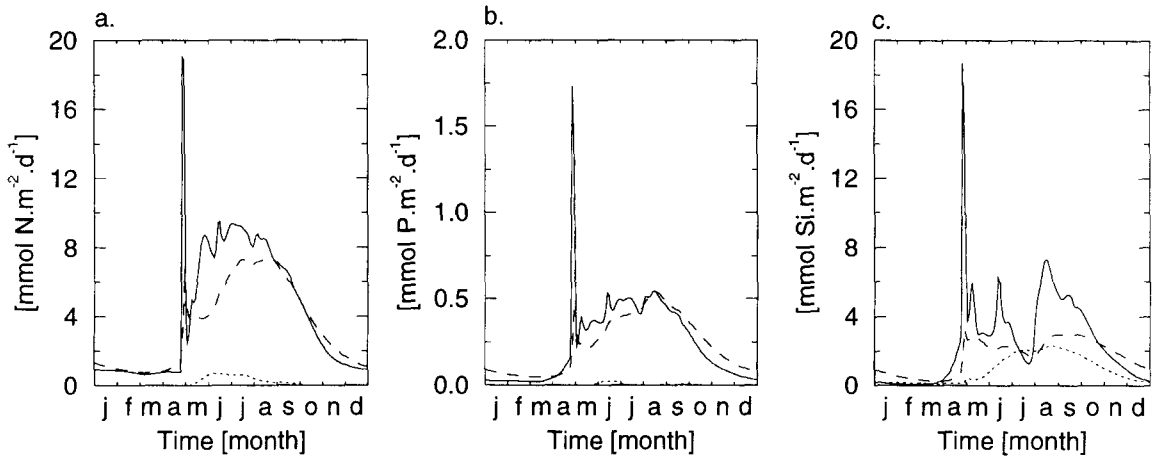

Fig. 14. a. The particulate input (solid line), the mineralization in the oxic layer (dashed line) and mineralization in the lower layers modelled with the ERSEM model in box 9 for nitrogen; b. for phosphate; c. for silicate.

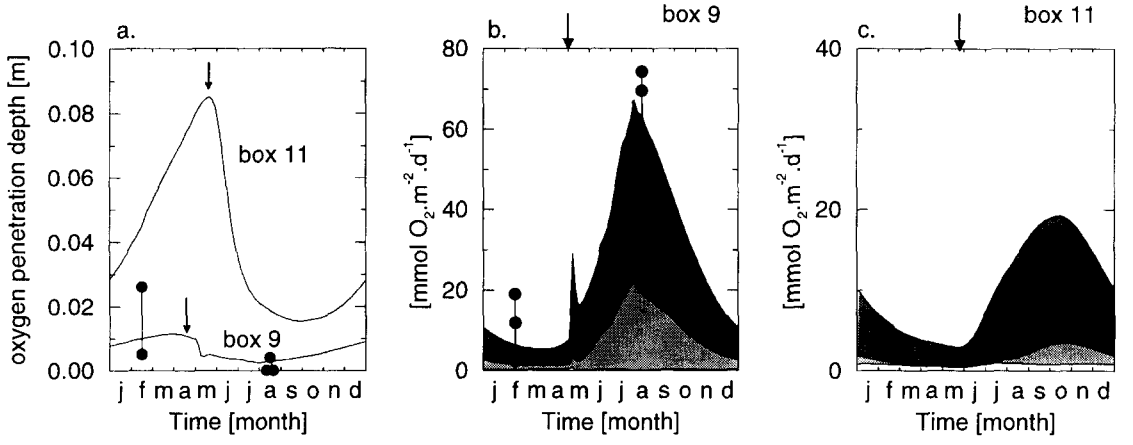

Fig. 15. Seasonal variation of a. oxygen penetration depth; b. the total oxygen consumption; c. idem for box 11 and the contribution of the three oxygen consuming processes in boxes 9 and 11: nitrification (white), oxidation of reduced materials (grey) and oxidation of organic material (dark grey). The arrows refer to the maximum of the spring bloom as simulated by the pelagic submodel (Varela *et al.*, 1995). The •'s refer to field observations by Lohse *et al.* (1993) at three stations in the German Bight (box 9).

caused by nitrification. The seasonal development of the nitrate profiles shows large differences between box 9 and 11 (Fig. 18). In box 9 nitrification causes maximum concentration at 1 to 3 cm depth just before deposition of the spring bloom when oxygen penetration depth is at maximum. From July to September nitrate is almost absent in the pore waters of this box. In box 11 highest nitrate concentrations are calculated for June-July when nitrification is stimulated by increasing ammonium production rates at still large enough oxygen penetration depths. According to the model nitrification is oxygen-limited in the coastal boxes and ammonium-limited in the northern boxes close to the ocean during summer.

In general the calculated concentrations of ammonium in the upper 5 cm agree fairly well with field data (Lohse *et al.*, 1993; Van Raaphorst *et al.*, 1990). Larger discrepancies between simulated and observed values occur in the deeper layers, particularly during summer. An example for box 9 is presented in Fig. 19. The February profile of nitrate (Fig. 20) is within the range of the field data. In August the observed nitrate profiles are lower than the simulated profiles probably due to the higher simulated ni-

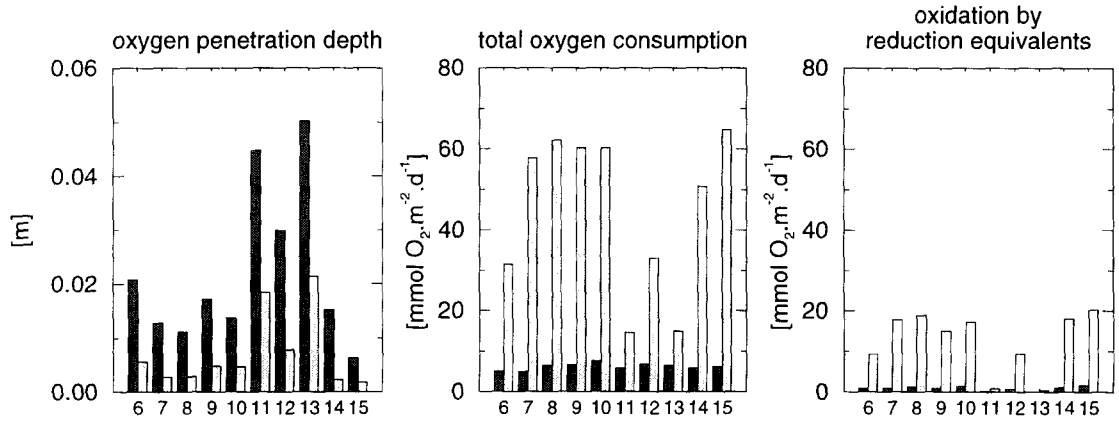

Fig. 16. a. annual mean oxygen penetration depths; b. total oxygen consumption; and c. oxygen consumption due to oxidation of reduced material for February (dark grey) and August (light grey).

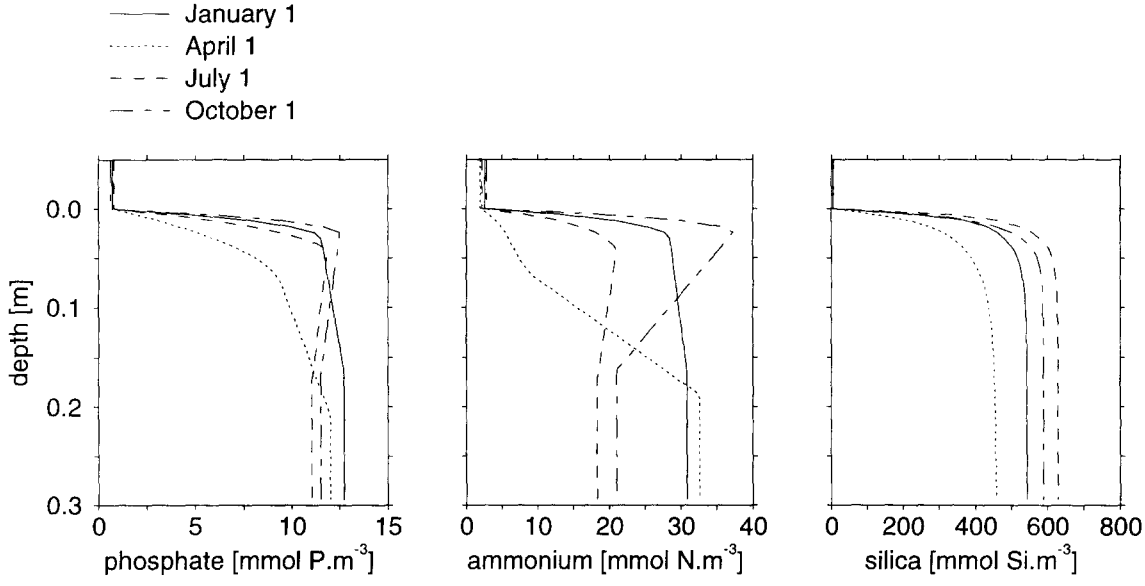

Fig. 17. Profiles for phosphate, ammonium and silica on 4 points in time as simulated for box 9.

trate concentrations in overlying water. The examples in Figs 19 and 20 demonstrate substantially different profiles measured within a single ERSEM box. This makes it almost impossible to fully compare the model with field observations.

The sediment-water exchange rates of dissolved nitrogen show a pronounced seasonal variation (Figs 21 and 23). The fluxes of nitrate and N_2 are suppressed in favour of ammonium during summer. The N_2 flux shows a similar pattern as nitrate, because the main source for denitrification is nitrate produced through nitrification. Nitrate and N_2 fluxes are at maximum in spring when O_2 penetrates deepest into the sediment. In April nitrate and N_2 contribute 25% and 85% to the total N flux in the boxes 9 and 11, respectively (Fig. 21).

Substantial parts of the ammonium produced through mineralization are nitrified to nitrate and subsequently denitrified. This holds particularly for the offshore boxes (11, 12 and 13) during winter. This result is in accordance with field observations of Van Raaphorst *et al.* (1992) and Lohse *et al.* (1993) who con-

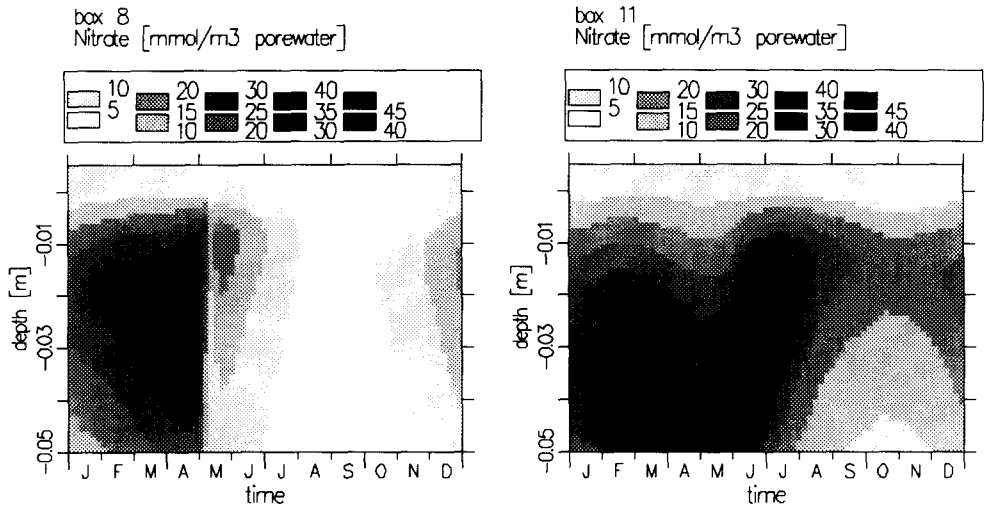

Fig. 18. Seasonal dynamics of profiles of nitrate as simulated for box 9 (left) and box 11 (right).

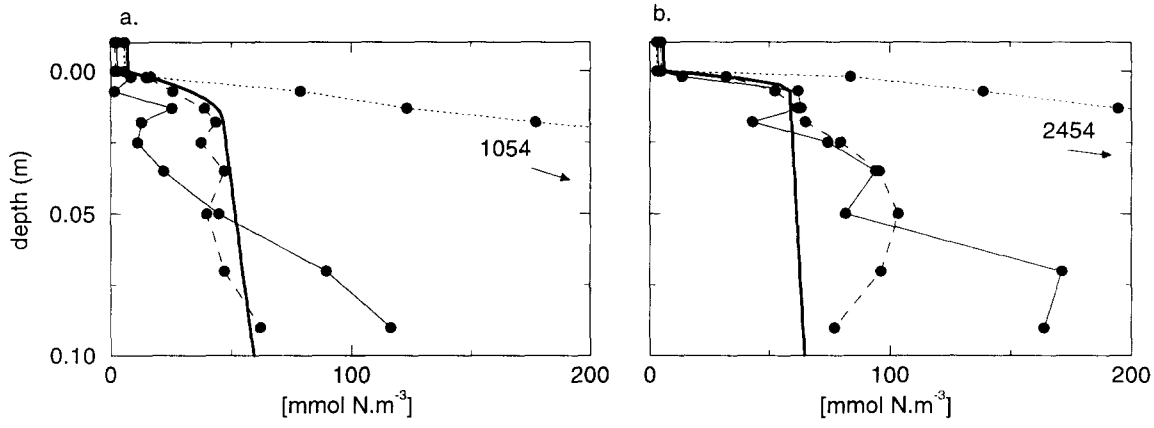

Fig. 19. Simulated NH_4^+profiles (thick solid line) and measured NH_4^+profiles at three stations (thin solid, dotted and dashed lines) for box 9 in a. February and in b. August. (Data from Lohse *et al.*, 1993).

cluded that nitrification and denitrification can dominate N-fluxes in non-eutrophied offshore sediments and that ammonium fluxes dominate in eutrophic coastal areas.

The simulated N-fluxes are compared with field observations of Lohse *et al.* (1993) in Figs 22 and 23. Again, the observations show large variations for most of the measured rates at different stations, demonstrating major heterogeneity within the ERSEM boxes in the field data.

Phosphate Production of phosphate and nitrogen is coupled to mineralization of organic carbon. Phosphate shows similar pore-water profiles as ammonium (Fig. 17). The low phosphate concentrations in the upper 5 mm observed in February are, however, not simulated by the model (Fig. 24a). The high pore-water concentrations observed at two stations in August are not reproduced by the model (Fig. 24b).

Subsurface gradients of phosphate are less pronounced than those of ammonium (Fig. 17). This is caused by the high adsorption distribution coefficient applied in the phosphate submodel, by which changes in phosphate concentration are buffered in the oxic layer. Fig. 25c indicates that the sorbed pool is largest in summer, but that phosphate is not stored over the season. This is also reflected by field observations (Slomp & Van Raaphorst, 1993a), especially if the (highest) values measured at Helgoland Bight are neglected as not representative for the entire area

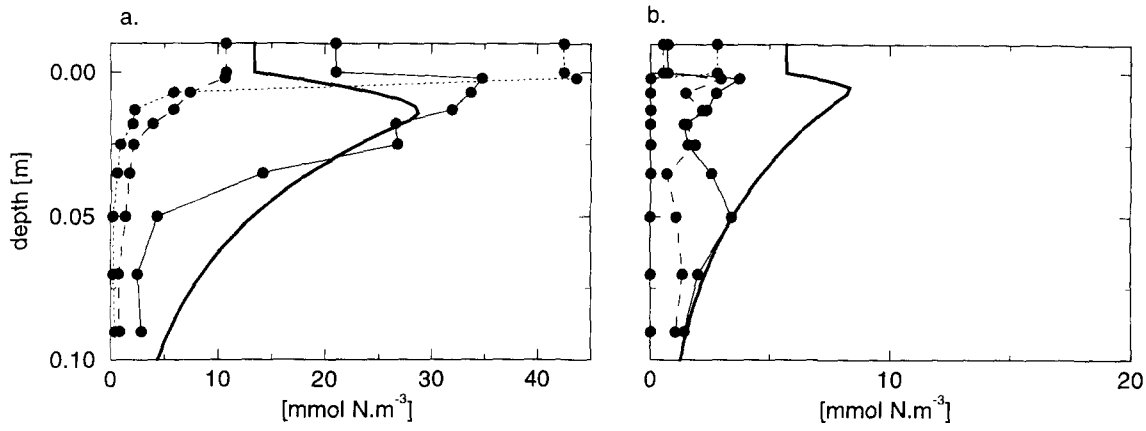

Fig. 20. Simulated NO_3^-profiles (thick solid line) and measured NO_3^-profiles at three stations (thin solid, dotted and dashed lines) for box 9 in a. February and b. August. (Data from Lohse *et al.*, 1993).

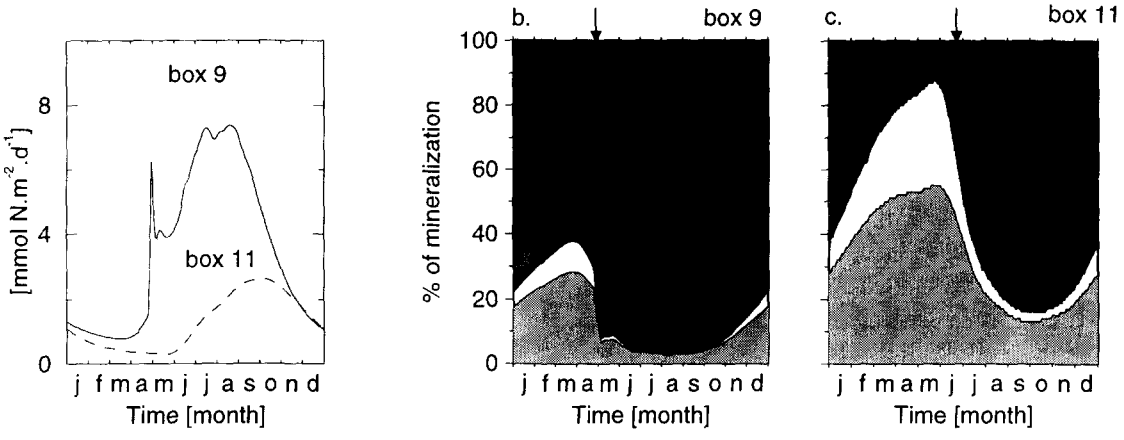

Fig. 21. a. Mineralization of N in boxes 9 and 11 (mmol $N \cdot m^{-2} d^{-1}$); b. the relative composition of sediment-water fluxes of nitrogen: ammonium (dark grey), N_2 (white) and nitrate (grey) for box 9 and c. idem for box 11. The arrows refer to the maximum of the spring bloom as simulated by the pelagic submodel (Varela *et al.*, 1995).

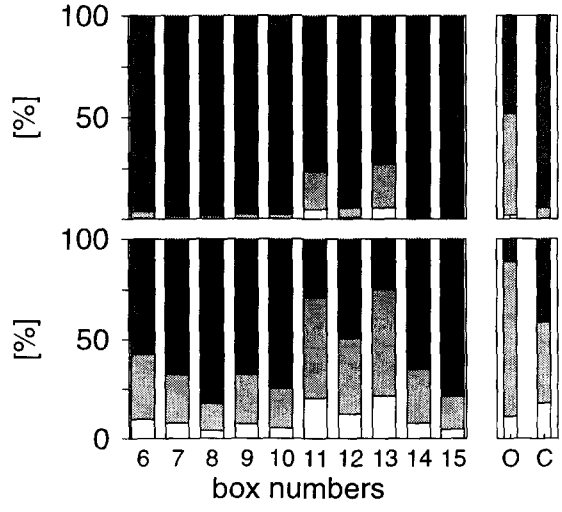

Fig. 22. Simulated annual relative simulated rates of N-mineralization (=100%), nitrification (white + light grey) and denitrification (white) compared with field data of Lohse *et al.* (1993) for offshore (o) and coastal (c) areas for February (lower graph) and August (upper graph).

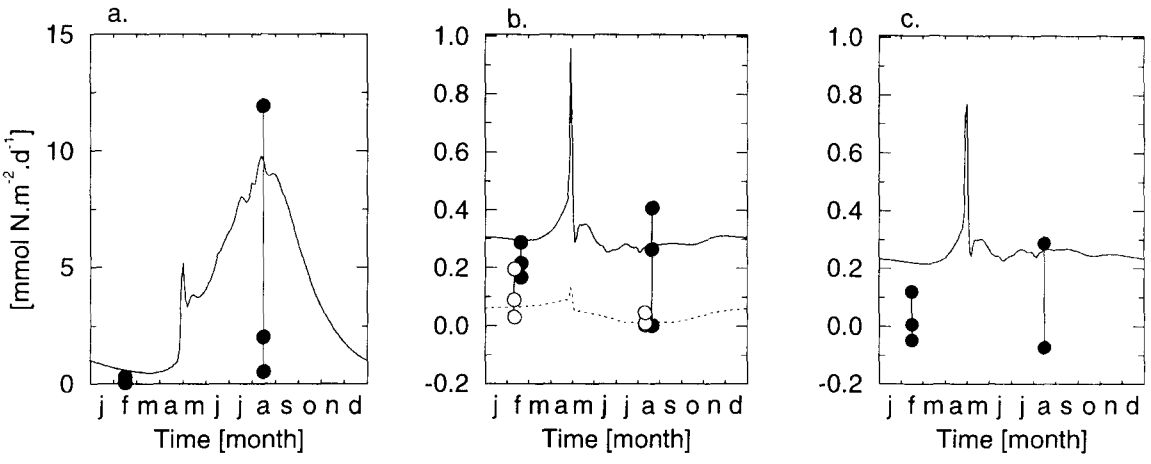

Fig. 23. Simulated seasonal dynamics of the N-fluxes for box 9 with field observations at three stations in the German Bight (•, Lohse *et al.* (1993)). (a) ammonium flux; (b) nitrification (solid line •) and denitrification (dotted line, ○), and (c) nitrate flux

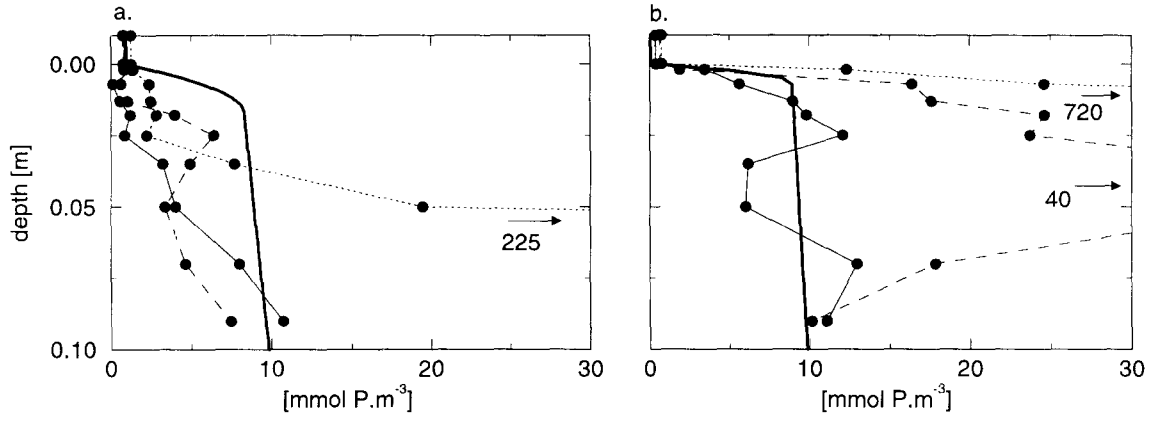

Fig. 24. Simulated phosphate profiles (thick solid line) and measured phosphate profiles at three stations (thin solid, dotted and dashed lines) for box 9 in a. February and b. August (data from Slomp, unpublished data).

(Lohse *et al.*, 1993).

The simulated fluxes of phosphate are within the range found by Slomp & Van Raaphorst (1993b).

Silicate The pore-water concentrations are lowest in April just before the deposition of the spring bloom. Highest concentrations are simulated for August-October (Fig. 17). The model did not reproduce the observed profiles in box 9 (Fig. 26). In general, the model calculates too high concentrations in the deeper layers of the sediment. The gradients at the sediment water interface and the simulated fluxes, however, fit fairly well with the field observations (Fig. 26).

7. DISCUSSION

Early diagenesis of nutrients is driven by mineralization of organic matter in the sediments (Froelich *et al.*, 1979). As a consequence modelling of benthic nutrient dynamics heavily depends on an accurate estimate of the deposition of organic matter on the sea floor. Also the quality of the organic matter in terms of degradability and carbon: nutrient ratios are of importance (Berner, 1980). In the present study deposition and organic matter composition are obtained from other submodels of the ERSEM model and not directly from field data. This means that our results depend on the other ERSEM submodels including their underlying assumptions and simplifications as well as

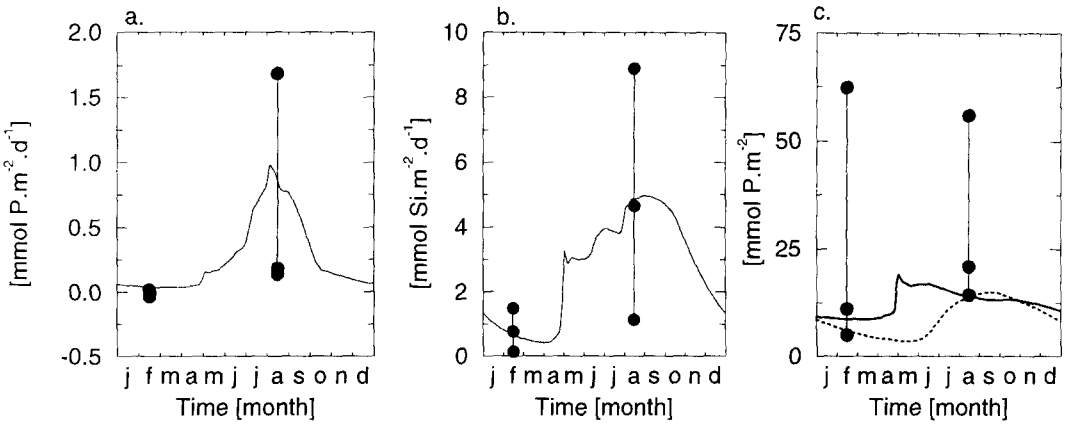

Fig. 25. a. Simulated seasonal dynamics of the P-flux; b. idem for Si-flux for box 9 with field observations at three stations in the German Bight; (•, field data from Slomp & Van Raaphorst, 1993a; Gehlen, 1993). c. Simulated seasonal dynamics of phosphate adsorbed in the upper 1 cm of the sediments for box 9 (solid line) and box 11 (dotted line) with field observations at three stations in the German Bight (Slomp), unpublished results).

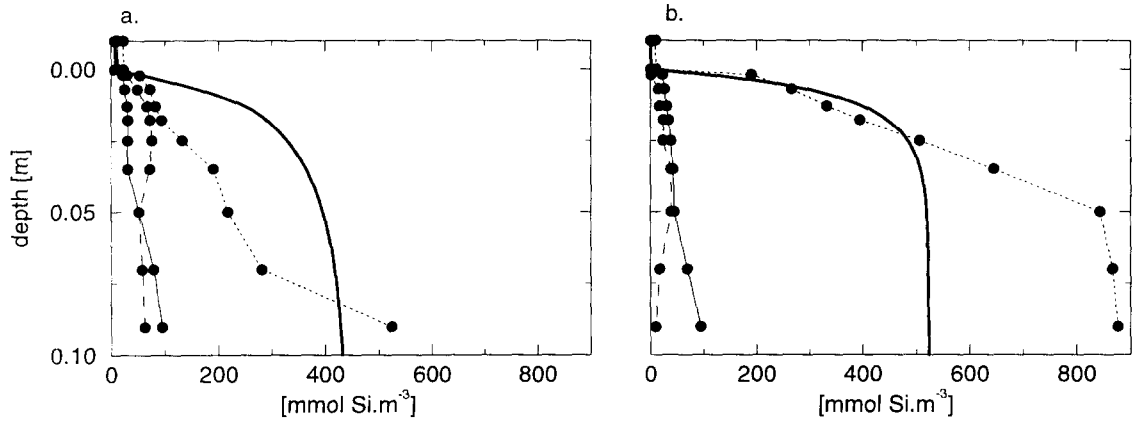

Fig. 26. Simulated silicate profiles (thick solid line) and measured silicate profiles at three stations (thin solid, dotted and dashed lines) for box 9 in a. February and b. August. (Data from Gehlen, 1993).

the associated uncertainties and errors. The advantage of this approach, however, is that the interactions between different compartments of the North Sea ecosystem can be evaluated within one single modelling framework (Baretta *et al.*, 1995), and that first estimates on the contribution of the sediments in overall nutrient cycling can be made for parts of the North Sea for which the amount of experimental data is insufficient.

The nutrient fluxes in box 9 are in the range of observations. It is questionable, however, whether the highest measured fluxes can be considered as representative for box 9 (Lohse *et al.*, 1993). Neglecting this observation would lead to the conclusion that the mineralization of N and P is too high in the model. Since the deposition of particulate material to the benthos and the total mineralization rates as indicated by the O_2 consumption are in the right order of magnitude, the conclusion must be either that the C/N and C/P ratios in the deposited material are too low or that the nutrients are preferentially buried or removed by the sediment.

In Fig. 28 the relative fluxes at the sediment-water interface, i.e. the fluxes divided by the yearly averaged mineralization, are given for boxes 9 and 11. In general the P-fluxes behave similarly as those of N, however with one important difference in box 9. Here the relative P-flux reaches substantially larger values than the N-flux in summer. This is explained by difference in adsorption properties of N and P. Phosphate is mod-

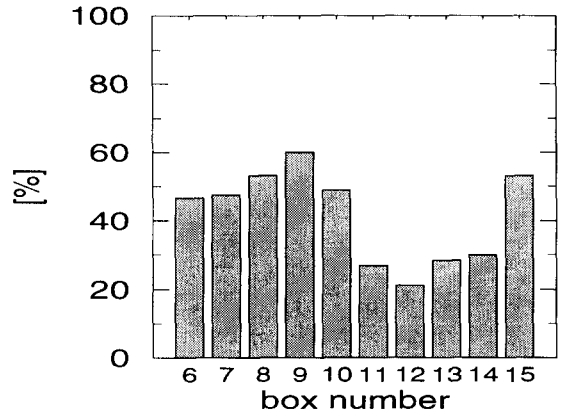

Fig. 27. The percentage of nitrogen taken up by primary producers and mineralized by the benthic system in the ERSEM boxes.

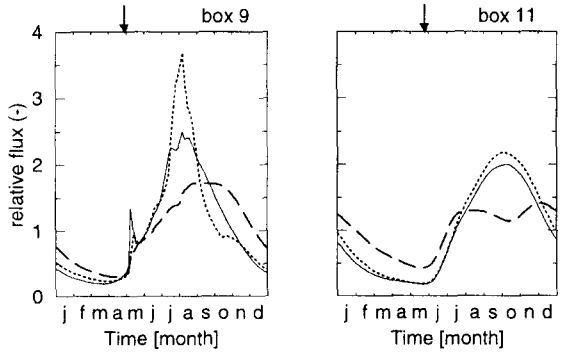

Fig. 28. The relative fluxes of N (solid), P (dotted) and Si (dashed) at the sediment-water interface for box 9 and box 11. The relative fluxes are calculated by dividing the actual flux by the yearly averaged mineralization in the sediment. The arrows refer to the point in time of the maximum of the spring bloom as simulated by the pelagic submodel.

elled as strongly buffered due to adsorption in the oxic and denitrification layer. If the oxygen and nitrate penetration decreases due to enhanced mineralization activity during summer, the adsorption capacity of the sediment decreases, resulting in higher pore-water concentrations and subsequently higher fluxes at the sediment-water interface. This phenomenon does not appear in box 11; here the concentration of nitrate remains much larger during summer.

The ratios between the nutrient fluxes differ only slightly between the boxes (Fig. 29), however with one dissimilarity for silica. Box 6 shows a distinctly larger Si/P ratio in the fluxes than the other boxes. This is caused by the different morphological properties of this box. In box 6 a deep but fully mixed water column exists and consequently the average light climate is less favourable than in the other boxes. Thus the primary production period is shorter. As a consequence the relative deposition of diatoms is larger than that of flagellates (Varela *et al.*, 1995).

The quality of the results depends on the mutual interference between all the different submodels. The overall picture of the relative importance of the benthic nutrient processes is a result of the dynamics of the whole model: the primary production process, all grazing processes, and all regeneration processes in the benthic and in the pelagic. The percentage of the primary production mineralized in the sediment varies between 20% in offshore boxes and 60% in coastal boxes (Fig. 27). Compared with estimations by Wollast (1991) (30 to 40%) and by Upton *et al.* (1993) (16 to 55 %) this is at the high side, particularly in the coastal boxes. Apparently, the nutrient input to the benthos as simulated by the model is too high.

Deposition of organic matter is directly coupled to local primary production in ERSEM. Effects of a possible sequence of deposition and erosion events (Jago *et al.*, 1993) by which particulate organic matter is gradually transported from *e.g.* the Southern Bight of the North Sea to the depocentres in the German Bight the and the Skagerrak (Eisma, 1987; Howarth *et al.*, 1993) are not included. Thus, typical differences observed in the field between nutrient dynamics in coarse-grained erosion areas and fine-grained deposition areas (Van Raaphorst *et al.*, 1992; Lohse *et al.*, 1993; Slomp & Van Raaphorst, 1993a) are only partly covered in our model.

Primary production seems adequately modelled in ERSEM. The spring bloom consists largely of diatoms which are assumed to settle on the sea floor when dissolved silica in the water column is depleted without substantial pelagic mineralization (Varela *et al.*, 1995). The resulting mass deposition at the end of the bloom forms the major input of biogenic silica to the sea floor and further contains both very labile and more refractory organic matter. The summer deposition mainly originates from flagellates which have gone partly through mineralization processes in the water column. As a result this material is less labile than the spring bloom deposition and contains only small amounts of biogenic silica (Varela *et al.*, 1995; Ebenhöh *et al.*, 1995). The effect of the spring bloom deposition is clearly recognized in the benthic oxygen consumption rates, the effluxes of ammonium and nitrate, and the nitrification and denitrification rates in the shallow coastal boxes (*e.g.* box 9 in the German Bight). The effect on the phosphate and silica fluxes is less pronounced due to the strong adsorption capacity of the oxic sediments for phosphate that buffers short-

term phosphate inputs, and because silica dissolution from diatom frustules is a relatively slow process. Thus, the silica effluxes during summer are caused by the dissolution of biogenic silica derived from the diatom deposition in spring.

Differences between the boxes are caused by water transport between the boxes and morphological properties of the boxes as depth and light climate. Joint & Pomroy (1993) report larger primary production for the ERSEM boxes 8 and 9 than for boxes 7 and 15 (Fig. 13). Our model, however, generates only small differences between these boxes. An unrealistic result of the model is the very high primary production in boxes 2/12 and 4/14. As a consequence the calculated deposition of organic matter in boxes 7 and 15 and probably also in boxes 12 and 14 is too high. Model results on nutrient fluxes from the sediment (Fig. 29c) in these boxes may thus also be too large.

To our knowledge, there are no reliable data to compare with the deposition of organic matter calculated by the ERSEM model. There are, however, several data sets on oxygen consumption by North Sea sediments. Cramer (1990), Van Raaphorst *et al.* (1992) and Nedwell *et al.* (1993) report oxygen consumptions by southern North Sea sediments between 10 and 75 mmol $O_2 \cdot m^{-2} \cdot d^{-1}$ during summer and less than 20 mmol $O_2 \cdot m^{-2} \cdot d^{-1}$ during winter. Annual carbon oxidation was estimated by these authors at 30 to 100 g $C \cdot m^{-2}$ of which according to Upton *et al.* (1993) 10 to 50% was performed by sulphate reduction. The results generated by our model compare well with these data. We conclude that on average input and mineralization of organic matter in the North Sea sediments are adequately modelled. In the ERSEM model, the North Sea is divided into ten large boxes. Obviously, in-box details and heterogeneity are lost by this schematization. In reality, however, substantial differences in sediment composition, organic matter deposition and nutrient early diagenesis can occur within a single box (Rutgers Van Der Loeff, 1980). Box 9 in the German Bight is a good example for this with coarse sands in the northern half and a deposition area with fine-grained sediments in the Helgoland Bight close to the Elbe Mouth (Wiesner *et al.*, 1990). These differences are reflected in the data points included in Fig. 23 to 26. The model can never reproduce these local variations and this makes detailed comparison with field data a difficult task. Still, the model seems to reasonably simulate box averaged oxygen and nutrient fluxes, at least for box 9 detailed data were available.

The modelled profiles of ammonium, nitrate and phosphate reflect non-steady state conditions in the sediments due to the seasonal variations of deposition of organic matter and changing nutrients concentrations in the overlying water. If compared with field observations the nutrient pore-water concentrations are fairly well modelled for the first 5 cm of the sediment for box 9 (Figs 19, 20 and 24). For the lower layers some discrepancies are observed, mainly caused by the absence of slowly degrading organic matter in the model (Ebenhöh *et al.*, 1995).

The phosphate profiles do not reflect the observed low concentrations in the upper few mm's in case of substantial adsorption in the oxic zone of the sediment (Sundby *et al.*, 1992; Slomp & Van Raaphorst, 1993b; Fig. 24). This is probably because the implementation of the adsorption process is too simple. The observed high phosphate concentration in August in box 9 is probably caused by small oxygen and nitrate penetration in the sediment in that period. Because the model does not predict such an anoxic state of the sediment the model results do not reflect these high phosphate pore-water concentrations. The simulation of silica profiles is still in a preliminary stage. The dependency of the silica dissolution on both solid biogenic and dissolved silica makes this submodel more complicated than those of the other nutrients. Even with the assumption of exponentially declining biogenic silica contents, the resulting computation scheme is not easily worked out (Appendix C.) and shows that our approximation method (steady states and correction sequence) has its limits. We were, however, able to simulate a clear response of the pore-water concentrations to the changing environmental conditions (deposition and temperature) and also obtained reliable Si-effluxes from the sediment.

The general picture that emerges from the model is depletion of organic matter and associated nutrient mineralization in winter and early spring. This conclusion is supported by field data obtained in the Southern Bight (Van Raaphorst *et al.*, 1992). Deposition of fresh organic matter after the spring bloom has dramatic effects on the nutrient processes in the sediment, with increased concentration and fluxes. Similar affects of spring bloom deposition were observed by Jensen *et al.* (1990) in Aarhus Bay. During summer, benthic nutrient cycling is driven by mineralization of organic matter deposited during spring and summer. In agreement with field observations (*e.g.* Van Raaphorst *et al.*, 1992), the model indicates that the greater part of the organic matter is mineralized within a single season. Build-up of organic matter and nutrients seems to be restricted to the few depostion areas in the North Sea.

Acknowledgements.— This research was partly funded

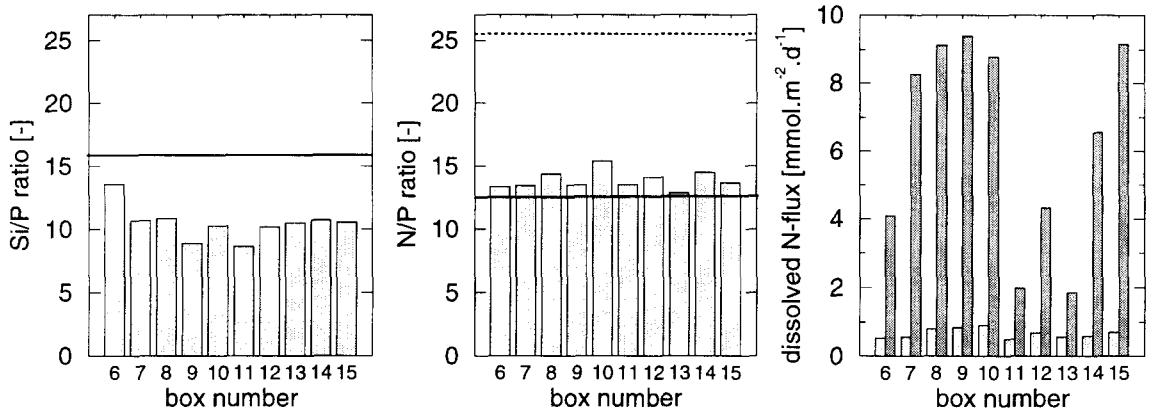

Fig. 29. a. Yearly averaged nutrient ratio of Si/P; b. idem of N/P in the ERSEM boxes and c. flux of dissolved inorganic N (nitrate + ammonium) in February (dark grey) and August (light grey). The solid and dotted lines in graphs a and b stand for the nutrient ratios applied in the model for diatoms and flagellates, respectively.

by the European Community under MAST contract number CT90-0021. Additional funds were supplied by BEON (proj. nr. NIOZ 92 E 03). Most field data were obtained from two BELS-cruises financially supported by the Netherlands Marine Research Foundation (grant 39104). We thank Leo Maas for mathematical advice during the development of the model.

REFERENCES

Abramowitz, M. & I.A. Stegun, 1964. Handbook of mathematical functions. Dover Publications, Inc., New York.

Aller, R.C., 1980. Diagenetic processes near the sediment-water interface of Long Island Sound I. Decomposition and nutrient geochemistry (S, N, P). –Adv.Geophys. **22:** 237–350.

Aller, R.C., J.E. Mackin, W.J. Ullman, W. Chen-You, T. Shing-Min, J. Jian-Cai, S. Yong-Nian & H. Jia-Zhen, 1985. Early chemical diagenesis, sediment-water solute exchange, and storage of reactive organic matter near the mouth of the Changjiang, East China Sea. –Cont. Shelf Res. **4:** 227– 251.

Baretta, J.W., W. Ebenhöh & P. Ruardij, 1995. The European Regional Seas Ecosystem Model, a complex marine ecosystem model. –Neth. J. Sea. Res. **33:** 233–246.

Baretta-Bekker, J.G., J. Baretta & E. Koch Rasmussen, 1995. The microbial food web in the European Regional Seas Ecosystem Model. –Neth. J. Sea. Res. **33:** 363–379.

Basford, D. & A. Eleftheriou, 1988. The Benthic Environment of the North Sea (56° to 61°N). –J. Mar. Biol. Ass. U. K. **68:** 125–141.

Berner, R.A., 1976. Inclusion of adsorption in the modelling of early diagenesis. –Earth planet. Sci. Letters **29:** 333–340.

Berner, R.A., 1980. Early diagenesis: A theoretical approach. Princeton Univ. Press, Princeton.

Billen, G., 1978. A budget of nitrogen recycling in North Sea sediments off the Belgian coast. – Estuar. coastal mar. Sci. **7:** 127–146.

Billen, G., 1982. An idealized model of nitrogen recycling in marine sediments. –Am. J. Sci. **282:** 512–514.

Blackford, J.C. & P.J. Radford, 1995. A structure and methodology for marine ecosystem modelling. – Neth. J. Sea. Res. **33:** 247–260.

Bouldin, D.R., 1968. Models for describing the diffusion of oxygen and other mobile constituents across the mud-water interface. –J. Ecol. **56:** 77–87.

Broecker, W.S. & T.H. Peng, 1973. Gas exchange between air and sea. –Tellus **26:** 21–35.

Broekhuizen, N., M.R. Heath, S.J. Hay & W.S.C. Gurney, 1995. Modelling the dynamics of the North Sea's mesozooplankton. –Neth. J. Sea. Res. **33:** 381–406.

Canfield, D.E., B.B. Jørgensen, H. Fossing, R. Glud, J. Gundersen, N.B. Ramsing, J.W. Hansen, L.P. Nielsen & P.O.J. Hall, 1993. Pathways of organic carbon oxidation in three continental margin sediments. –Mar. Geol. **113:** 27–40.

Carslaw, H.S. & J.C. Jaeger, 1946. Conduction of heat in solids. Oxford University Press, London.

Cramer, A., 1990. Seasonal variation in benthic metabolic activity in a frontal system in the North Sea. In: M. Barnes & R.N. Gibson., Trophic relationships in the marine environments. Aberdeen

Univ. Press, Aberdeen: 54–76.
Ebenhöh, W., C. Kohlmeier & P.J. Radford, 1995. The benthic biological submodel in the European Regional Seas Ecosystem Model. –Neth. J. Sea. Res. **33:** 423–452.
Eisma, D., 1987. The North Sea: an overview. –Phil. Trans. R. Soc. **316:** 461–485.
Fanning, K.A. & M.E.Q. Pilson, 1971. Interstitial Silica and pH in Marine Sediments: Some Effects of Sampling Procedures. –Science **173:** 1228–1231.
Fransz, H.G., J.P. Mommaerts & G. Radach, 1991. Ecological modelling of the North Sea. –Neth. J. Sea. Res. **28:** 67–140.
Froelich, P.N., G.P. Klinkhammer, M.L. Bender, N.A. Luedtke, G.R. Heath, D. Cullen, P. Dauphin, D. Hammond, B. Hartman & V. Maynard, 1979. Early oxidation of organic matter in pelagic sediments of the eastern equatorial Atlantic: suboxic diagenesis. –Geochim. cosmochim. Acta **43:** 1075–1090.
Gehlen, M., 1993. Fluxes of dissolved silica across the sediment-water interface. In: W. Van Raaphorst & J.P. Boon, The Integrated North Sea Programme 1991-1992, preliminary results, NIOZ-report 9. NIOZ, Texel.
Gehlen, M. & W. Van Raaphorst, 1993. Early diagenesis of silica in sandy North Sea sediments: quantification of the solid phase. –Mar. Chem. **42:** 71–83.
Gehlen, M., W. Van Raaphorst & R. Wollast, 1993. Kinetics of silica sorption on North Sea sediments. –Chem. Geol. **107:** 359–361.
Goloway, F. & M. Bender, 1982. Diagenetic models of interstitial nitrate profiles in deep sea sediments. –Limnol. Oceanogr. **27:** 624–638.
Henriksen, K. & W.M. Kemp, 1988. Nitrification in estuarine and coastal marine environments. In: T.H. Blackburn & J. Sørensen, Nitrogen cycling in coastal marine environments, SCOPE 33. Wiley & Sons, New York: 207–249.
Himmelblau, D.M., 1964. Diffusion of dissolved gases in liquids. –Chem. Rev. **64:** 527–550.
Howarth, M.J., K.R. Dyer, I.R. Joint, D.J. Hydes, D.A. Purdie, H. Edmonds, J.E. Jones, R.K. Lowry, T.J. Moffat, A.J. Pomroy & R. Proctor, 1993. Seasonal cycles and their spatial variability. –Phil. Trans. R. Soc. **343:** 383–402.
Hurd, D.C., 1973. Interaction of biogenic opal, sediment and seawater in the central equatorial Pacific. –Geochim. cosmochim. Acta **37:** 2257–2282.
Iler, R.K., 1979. The Chemistry of Silicate. John Wiley & Sons, New York.
Jago, C.F., A.J. Bale, M.O. Green, M.J. Howarth, S.E. Jones, I.N. McCave, G.E. Millward, A.W. Morris, A.A. Rowden & J.J. Williams, 1993. Resuspension processes and seston dynamics, southern North Sea. –Phil. Trans. R. Soc. **343:** 475–488.
Jahnke, R.A., S.R. Emerson & J.W. Murray, 1982. A model of oxygen reduction, denitrification and organic matter mineralization in marine sediments. –Limnol. Oceanogr. **27:** 610–623.
Jenkins, M.C. & W.M. Kemp, 1984. The coupling of nitrification and denitrification in two estuarine sediments. –Limnol. Oceanogr. **29:** 609–619.
Jensen, M.H., E. Lomstein & J. Sørensen, 1990. Benthic NH_4^+ and NO_3^- flux following sedimentation of a spring phytoplankton bloom in Aarhus Bight, Denmark. –Mar. Ecol. Prog. Ser. **61:** 87–96.
Joint, I. & A. Pomroy, 1993. Phytoplankton biomass and production in the southern North Sea. –Mar. Ecol. Prog. Ser. **99:** 169–182.
Jørgensen, B.B., 1989. Sulphate reduction in marine sediments from the Baltic Sea-North Sea transition. –Ophelia **31:** 1–15.
Krom, M.D. & R.A. Berner, 1980. The diagenesis of phosphorus in a nearshore marine sediment. –Geochim. cosmochim. Acta **45:** 207–216.
Laima, M.J.C., 1992. Extraction of seasonal variation of NH^+ pools in different types of coastal marine sediments. –Mar. Ecol. Prog. Ser. **92:** 75–84.
Lawson, D.S., D.C. Hurd & H.S. Pankratz, 1978. Silica dissolution rates of decomposing phytoplankton assemblages at various temperatures. –Am. J. Sci. **278:** 1373–1393.
Lenhart, H.J., G. Radach, J.O. Backhaus & T. Pohlmann, 1995. Simulations of the North Sea circulation, its variability, and its implementation as hydrodynamical forcing in ERSEM. –Neth. J. Sea. Res. **33:** 271–299.
Li, Y.H. & S. Gregory, 1974. Diffusion of ions in seawater and deep-sea sediments. –Geochim. cosmochim. Acta **38:** 703–714.
Lohse, L., J.F.P. Malschaert, C.P. Slomp, W. Helder & W. Van Raaphorst, 1993. Nitrogen cycling in North Sea sediments: interaction of denitrification and nitrification in offshore and coastal areas. –Mar. Ecol. Prog. Ser. **101:** 283–296.
Mackin, J.E. & R.C. Aller, 1984. Ammonium adsorption in marine sediments. –Limnol. Oceanogr. **29:** 250–257.
Malschaert, J.F.P. & W. Van Raaphorst, 1993. North Sea nutrient cycling: benthic pools of ammonium. In: W. Van Raaphorst & J.P. Boon, The Integrated North Sea Programme 1991-1992, preliminary results, NIOZ-report 9. NIOZ, Texel: 27–30.
Nedwell, D.B., R.J. Parker, A.C. Upton & D.J. Assinder, 1993. Seasonal fluxes across the sediment-water interface, and processes within sediments.

–Phil. Trans. R. Soc. **343:** 519–531.

Peterson, B.J., 1980. Aquatic primary productivity and the ^{14}C-CO_2 method: a history of the productivity problem. A. –Rev. Ecol. Syst. **11:** 359–389.

Press, W.H., B.P. Flannery, S.A. Teukolsky & W.T. Vetterling, 1986. Numerical Recipes . The art of Scientific Computing. Cambirdge University Press, Cambridge.

Rutgers Van Der Loeff, M.M., 1980. Nutrients in the interstitial waters of the Southern Bight of the North Sea. –Neth. J. Sea. Res. **14:** 144–171.

Schink, D.R., N.L. Guinasso & K.A. Fanning, 1975. Processes affecting the concentration of silica at the sediment-water interface of the Atlantic Ocean. –Geophys. Res. **80:** 3013–3031.

Slomp, C.P. & W. Van Raaphorst, 1993a. Forms of phosphorus in North Sea sediments and fluxes across the sediment-water interface. In: W. Van Raaphorst & J.P. Boon, The Integrated North Sea Programme 1991-1992, preliminary results, NIOZ-report 9. NIOZ, Texel: 20–23.

Slomp, C.P. & W. Van Raaphorst, 1993b. Phosphate adsorption in oxidized marine sediments. –Chem. Geol. **107:** 477–480.

Sundby, B., V. Gobeil, N. Silverberg & A. Muccu, 1992. The phosphorus cycle in coastal marine sediments. –Limnol. Oceanogr. **37:** 1129–1145.

Ullman, W.J. & R.C. Aller, 1982. Diffusion coefficients in nearshore marine sediments. –Limnol. Oceanogr. **27:** 552–556.

Upton, A.C., D.B. Nedwell, R.J. Parkes & S.M. Harvey, 1993. Seasonal benthic microbial activity in the southern North Sea; oxygen uptake and sulphate reduction. –Mar. Ecol. Prog. Ser. **101:** 273–281.

Van Raaphorst, W., H.T. Kloosterhuis, E.M. Berghuis, A.J.M. Gieles, J.F.P. Malschaert & G.J. Van Noort, 1992. Nitrogen cycling in two types of sediments of the southern North Sea (Frisian Front, Broad Fourteens): field data and mesocosm results. –Neth. J. Sea. Res. **28:** 293–316.

Van Raaphorst, W., H.T. Kloosterhuis, A. Cramer & K.J.M. Bakker, 1990. Nutrient early diagenesis in the sandy sediments of the Dogger Bank area, North Sea: pore water results. –Neth. J. Sea. Res. **26:** 25–52.

Van Raaphorst, W., P. Ruardij & A.G. Brinkman, 1988. The assessment of benthic phosphorus regeneration in an estuarine ecosystem model. –Neth. J. Sea. Res. **22:** 23–36.

Vanderborght, J.P. & G. Billen, 1975. Vertical distribution of nitrate concentration in interstitial water of marine sediments with nitrification and denitrification. –Limnol. Oceanogr. **20:** 953–961.

Vanderborght, J.P., R. Wollast & G. Billen, 1977a. Kinetic models of diagenesis in disturbed sediments. Part 2. Nitrogen diagenesis. –Limnol. Oceanogr. **22:** 794–803.

Vanderborght, J.P., R. Wollast & G. Billen, 1977b. Kinetic models of diagenesis in disturbed sediments. Part 1. Mass transfer properties and silica diagenesis. –Limnol. Oceanogr. **22:** 787–793.

Varela, R.A., A. Cruzado & J.E. Gabaldón, 1995. Modelling primary production in the North Sea using the European Regional Seas Ecosystem Model. –Neth. J. Sea. Res. **33:** 337–361.

Wiesner, M.G., B. Haake & H. Wirth, 1990. Organic facies of surface sediments in the North Sea. –Org. Geochem. **15:** 419–432.

Wollast, R., 1991. The coastal organic carbon cycle: fluxes, sources and sinks. In: R.F.C. Mantoura, J.M. Martin, & R. Wollast, Ocean margin processes in global change, physical, chemical, and earth sciences reports 9. John Wiley & Sons, Chicester: 365–381.

APPENDIX A.
approximation of the transient profiles and fluxes

The estimation of the adaptation time t_a is based on the general solution of Eq. 2. By substituting $\xi = C - \frac{M}{k}$ Eq. 2 becomes:

$$\frac{\partial \xi}{\partial t} = D\frac{\partial^2 \xi}{\partial z^2} - k\xi \tag{13}$$

If the steady-state solution of Eq. 13 is taken as the initial condition, say $f(z)$, and if $g(z)$ is the new profile after changing the boundary condition at $t = 0$, the general solution is (Carslaw & Jaeger, 1946):

$$\xi(z,t) = g(t) + \frac{2}{H}\sum_{n=1}^{\infty} b_n e^{-t(k+Dn^2\pi^2)} \sin(n\pi z) \tag{14}$$

in which

$$b_n = \int_{z'=0}^{H} [f(z') - g(z')] \sin(n\pi z') dz' \tag{15}$$

The second term in Eq. 14 fully describes the transient state of ξ and thus of C. The dynamics are determined by the exponential terms.

The adaptation time is defined from Eq. 14. Taking as criterion the first term in the series and thus neglecting the higher order terms of Eq. 14) the adaptation time is approximated by:

$$t_a = \frac{p+1}{k + \pi^2 DH^{-2}} \tag{16}$$

This adaptation time is applied in the following way:

$$F(t + \Delta t) = G(z) + [F(z) - G(z)]e^{-\frac{\Delta t}{t_a}} \tag{17}$$

in which $F(z, t + \Delta t)$ is the concentration present at $t + \Delta t$ at depth z, $F(z)$ is the concentration at depth z the concentration present at t and $G(z)$ the concentration to be obtained for large values of Δ t.

However in the model we are not interested in concentrations at a time $t + \Delta t$ but in the 'average' profile during a time step. Thus, the average concentration during the time interval $[t, t + \Delta t]$ is calculated as:

$$\overline{F(t \Rightarrow t + \Delta t)} = G(t) + [F(z) - G(z)]\frac{t_a}{\Delta t}(1 - e^{-\frac{\Delta t}{t_a}}) \tag{18}$$

In which the bar over F denotes the time-step averaged profile. From this profile all fluxes and depth-integrated concentrations are calculated.

APPENDIX B.
dynamical solutions

In section 3. two exact dynamical solutions of partial differential equations (PDE's) are applied to compare with the appoximate solutions of the model (Carslaw & Jaeger, 1946). In both cases the solutions are valid of Eq. 2 in which $p = 0$:

$$\frac{\partial C}{\partial t} = D\frac{\partial^2 C}{\partial z^2} - kC + M \tag{19}$$

B.1. PDE WITH ZERO-ORDER INPUT AND FIRST ORDER LOSS TERM

By substituting $\xi = C - \frac{M}{k}$ Eq. 19 becomes:

$$\frac{\partial \xi}{\partial t} = D\frac{\partial^2 \xi}{\partial z^2} - k\xi \tag{20}$$

if the following conditions are fulfilled:
- Mineralization takes place in a finite layer $0 < z < H$.
- Initial constant gradient: ξ_{in} $(0 < z < H)$
- Ends at concentration ξ_0 and ξ_H, respectively at $z = 0$ and $z = H$.

the dynamical solution of Eq. 20 is:

$$\xi(z,t) = \frac{2}{H}\sum_{n=1}^{\infty} e^{-t(Dn^2\pi^2H^{-2}+k)}\sin(n\pi z)\left\{\xi_{in}(1-\cos(n\pi H))\frac{n\pi D}{H} + \int_{\lambda=0}^{t} e^{\lambda(Dn^2\pi^2H^{-2}+k)}(\xi_0 - (-1)^n\xi_H)\,d\lambda\right\} \tag{21}$$

B.2. PDE WITH ZERO-ORDER INPUT

If the following conditions are fulfilled:
- Mineralization takes place in a finite layer $0 < z < H$.
- The surface concentration $C(0) = 0$ for $t \geq 0$
- Initial constant gradient: C_{in} $(0 < z < \infty)$

the dynamical solution of Eq. 19 with $k = 0$ becomes:

$$C(z,t) = C_{in}\,\mathrm{erf}\frac{z}{2\sqrt{Dt}} + Mt\left\{1 - 4\,\mathrm{i}^2\mathrm{erfc}\frac{z}{2\sqrt{Dt}} + 2\,\mathrm{i}^2\mathrm{erfc}\frac{H+z}{2\sqrt{Dt}} - 2\,\mathrm{i}^2\mathrm{erfc}\frac{H-z}{2\sqrt{Dt}}\right\} \tag{22}$$

APPENDIX C.
general steady-state solutions

The solutions of the steady-state equations of the partial differential equations (PDE's) are given only in general terms without explicit formulations of the integration constants. The latter are calculated in the model by a Gauss-elimination method.

C.1. AMMONIUM

The steady-state solutions for the set of PDE's listed in textbox 1 for ammonium are:

$$\begin{aligned} A_1(z) &= a_{11}e^{-\gamma z} + a_{12}e^{\gamma z} + a_{15} \\ A_2(z) &= a_{21}e^{-\alpha\zeta} + a_{24}z + a_{25} \end{aligned}$$

in which
$a_{11}, a_{12}, a_{24}, a_{25}$ are integration constants, and

$$\begin{aligned} a_{15} &= \frac{M_A}{k} \\ a_{21} &= \frac{M_A}{D_A\alpha^2} \\ \gamma &= \sqrt{\frac{k}{D_A}} \end{aligned}$$

C.2. NITRATE

The steady-state solutions for the set of PDE's listed in textbox 1 for nitrate are:

$$\begin{aligned} N_1(z) &= n_{11}e^{-\gamma z} + n_{12}e^{\gamma z} + n_{13}z^2 + n_{14}z + n_{15} \\ N_2(z) &= n_{21}e^{-\beta z} \end{aligned}$$

in which n_{14} and n_{21} are integration constants and

$$\begin{aligned} n_{11} &= \frac{a_{11}}{D_N\gamma^2} \\ n_{12} &= \frac{a_{12}}{D\gamma^2} \\ n_{13} &= \frac{a_{15}}{2D} \\ n_{15} &= N_0 - n_{11} - n_{12} \\ \beta &= \sqrt{\frac{d}{D_N}} \end{aligned}$$

γ, a_{11}, a_{12} and a_{15} are listed in the ammonium model. See C.1.

C.3. PHOSPHATE

The steady-state solutions for the set of PDE's listed in textbox 2 are:

$$\begin{aligned} P_1(z) &= p_{13}z^2 + p_{14}z + p_{15} \\ P_2(z) &= p_{21}e^{-\alpha\zeta} + p_{24}z + p_{25} \\ P_3(z) &= p_{31}e^{-\alpha\zeta} + p_{35} \end{aligned}$$

in which p_{14}, p_{24}, p_{25} and p_{35} are integration constants, and

$$\begin{aligned} p_{13} &= P_0 \\ p_{13} &= \frac{M_P}{2D_P} \\ p_{21} &= \frac{M_P}{D_P\alpha^2} \\ p_{31} &= \frac{M_P}{e}^{-\alpha(z_{an}-z_{ox})} D_P\alpha^2 \end{aligned}$$

C.4. SILICATE

The steady-state solutions for the set of PDE's listed in textbox 3 are:

$$\begin{aligned} C_1(z) &= c_{13}z^2 + c_{14}z + c_{15} \\ C_2(z) &= c_{21}I_0(\lambda e^{-\frac{1}{2}\beta\zeta}) \end{aligned}$$

in which c_{13}, c_{14} and c_{21} are integration constants and

$$\begin{aligned} c_{15} &= \frac{sB_1}{2D_{Si}} \\ \lambda &= \frac{2}{\beta}\frac{sB_1}{Si_\infty D_{Si}} \end{aligned}$$

I_0 stands for the modified Bessel function of 0th order.

C.5. REDUCTION EQUIVALENTS

The steady-state solutions for the set of PDE's listed in textbox 4 are:

$$\begin{aligned} R_1(z) &= r_{13} z^2 \\ R_2(z) &= r_{21} e^{-\alpha\zeta} + r_{22} e^{-\beta z} + r_{25} \end{aligned}$$

in which r_{25} is an integration constant and

$$\begin{aligned} r_{13} &= \frac{M_r}{2D_R} \\ r_{21} &= \frac{M_O}{\eta_r D_R \alpha^2} \\ r_{22} &= -\frac{dn_{21}}{D_R \beta^2} \end{aligned}$$

The definitions of β, n_{21} are given in the nitrate model (C.2).

C.6. OXYGEN

The steady-state solution for the differential equation listed in textbox 5 is:

$$Ox(z) = o_{13} z^2 + o_{14} z + n_{15}$$

in which o_{13} and o_{14} are integration constants and

$$o_{15} = Ox_0$$